The Creep Behaviour of Rubbers Reinforced with Particulate or Short Fibres

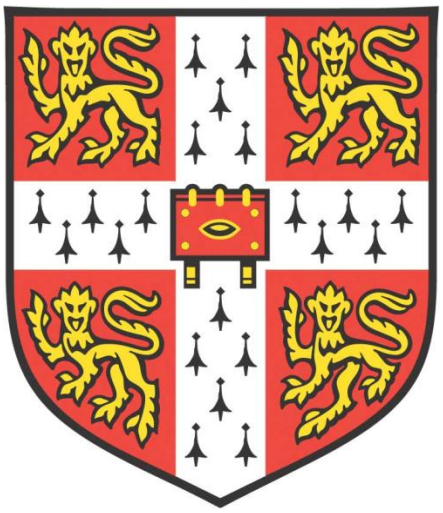

Yi Cui

Downing College

Department of Materials Science and Metallurgy

University of Cambridge

This dissertation is submitted for the degree of Doctor of Philosophy

September 2021

Preface

This dissertation is submitted for the degree of Doctor of Philosophy at the University of Cambridge. All the observations, results and conclusions presented here are my own work from October 2017 to September 2021, under the supervision of Professor T.W. Clyne in the Department of Materials Science and Metallurgy at the University of Cambridge.

I hereby declare that this dissertation is neither the same as any work of others nor is being submitted for any other degree or diploma or qualification at the University of Cambridge or any other university or institution. I emphasise that all results in this dissertation are my own work and include nothing which is derived from others. It is fewer than 60,000 words in length.

Yi Cui

Abstract

The Creep Behaviour of Rubbers Reinforced with Particulate or Short Fibres

Yi Cui

Elastic stress-strain testing and (primary and secondary) creep testing have been carried out on unfilled polyurethane rubber and two rubber composites filled with 10 vol% and 20 vol% alumina particulates. They have been run at three different temperatures (20°C, 45°C and 65°C) for all three materials. The stress-strain curves of the rubber conformed well to the expectation of the conventional rubber elasticity theory. Furthermore, the true stress-strain plots of those three materials exhibited an approximately linear relationship with stiffness increasing by adding the particulates: the relationships conformed to the composite elastic theory. In order to capture the creep historical strain of these materials with an uncomplicated method, a Miller-Norton empirical formulation, which is conventionally used for predicting the creep behaviour of metal materials, is adapted in this work. The creep behaviour of all three materials could be captured well by using the Miller-Norton constitutive law and the observed dependence on temperature has been used to estimate the activation energy for creep to be ~ 7 kJ $mole^{-1}$. This showed that the creep process did not involve rupture of covalent bonds (for the range of applied loads used) but was associated with physical processes such as molecular untangling. The fillers enhanced the creep resistance, to a degree that was quantitatively consistent with the expected load transfer between matrix and particulate.

After these results, the particulates in polyurethane rubber were replaced by different amounts (5 vol% and 10 vol%) of alumina short fibres. The tensile stress-strain testing and the fixed load creep testing of these fibrous reinforced composite rubbers were done at the same temperatures (20°C, 45°C and 65°C). The samples were made via

a blending and extrusion process that produced a degree of fibre alignment along the axial loading direction. Prior milling procedures were used to produce fibres with two different average aspect ratios, which were estimated to be about 10 and 16. True stress-strain relationship from these fibrous reinforced composite rubbers also exhibited approximately linear plots. The dependence of stiffness on the volume fraction and the fibre aspect ratio conformed well to the predictions from the Eshelby model. Also, the creep behaviour of all the materials could be captured well by using the Miller-Norton constitutive law with the average matrix stress predicted from the Eshelby model. Thus, it could be seen short fibres were much more effective for reducing creep rate than particulates.

To check the agreement of another fibrous reinforced composite rubber with the Eshelby model and the Miller-Norton constitutive law, tensile stress-strain testing and creep testing have also been carried out on silicone rubber, Dow Corning SE 1700, with and without short fibrous alumina reinforcement at two temperatures (20°C and 65°C). It was found that silicone rubber alone is stiffer and shows greater creep resistance than polyurethane rubber alone. Furthermore, when silicone rubber was substituted for polyurethane rubber as the matrix in fibrous composite, its greater stiffness significantly reduced creep strain.

Acknowledgements

Many thanks are due to my sponsor, AWE, and both Dr. Mogon Patel and Dr. Kevin Hunt for the opportunity to study for this degree.

Also, heartfelt thanks to Downing College Alumnus, Prof. Peter Thrower and his wife, Carol Thrower, who helped me out with the Thrower Funding throughout the time of my thesis writing.

In particular I would like to thank my supervisor, Prof. Bill Clyne, for his guidance and support throughout this work. I believe that I couldn't have completed this without him.

I sincerely thank Dr. James Dean, Dr. Jimmy Campbell, Dr. Max Burley and Mr Bob Stearn for their help, training, and advice in my thesis and with the practical work at Cambridge. Thanks also to the colleagues in Gordon Lab for their advice, suggestions, and discussions.

Many thanks to Mr Alistair Grearson, who led me into the field of materials science at Sandvik Hard Materials, for proof-reading my work.

I wish to thank my family, especially my wife, Neringa, for their support during my study over the last four years. I could not have achieved this without you.

Finally, I would like to thank all my friends and colleagues at department of Material Science and Metallurgy, Cambridge, who have helped me during my study.

Contents

Nomenclature

Roman Symbols

A		Constant
A	$MPa^{-n}\ s^{-(m+1)}$	Miller-Norton Constant
C	Pa	Stiffness (tensor of fourth rank)
C	$MPa^{-n}\ s^{-(m+1)}$	Miller-Norton Multiplier
d	mm	inclusion diameter
E	Pa	Young's Modulus
f	-	reinforcement (fibre) volume fraction
G(t)	Pa	Time dependent shear modulus
G_0	Pa	Initial shear modulus
g_g	-	Dimensionless shear relaxation modulus
g_i	-	Material constants
I	-	unit tensor (identity matrix)
k	$J\ mol^{-1}K^{-1}$	Boltzmann Constant
l	mm	Extended Length of Rubber
l	mm	inclusion length
m	-	Dimensionless Constant
n	m^{-3}	Number of Chain Segment
n	-	Steady-State Creep Exponent
Q	$kJ\ mol^{-1}$	Activation Energy
R	$J\ mol^{-1}K^{-1}$	Universal Gas Constant
S	-	Eshelby tensor
s	-	fibre aspect ratio

T	K	Absolute Temperature
t	s	Time

Greek Symbols

ε	-	Strain
$\dot{\varepsilon}$	s^{-1}	Strain Rate
λ	-	Extension Ratio
ν		Poisson's Ratio
ρ	kg m^{-3}	Density
σ	Pa	Stress
τ_i	s	Relaxation time

Subscripts

0	initial
c	composite
cr	creep
f	fibre (reinforcement)
g	global
g	glass transition
GB	Grain Boundary Diffusion
i	interfacial
m	matrix
m	melting
N	Nominal
s	Secondary or Steady-State of Creep
SD	Self Diffusion
T	True
Y	Yield

Acronyms

BSE	Back-Scattered Electron
LVDT	Linear Variable Differential Transformer
MMCs	Metal Matrix Composites
M-N	Miller-Norton

PDMS	Polydimethylsiloxane
PU	Polyurethane
SEM	Scanning Electron Microscopy

Chapter 1

Introduction

1.1 Background

The creep behaviour of rubber has been studied for over several decades [1-5]. There are many practical situations and applications, for example, where rubbers are used for various seals, connectors, damping systems, etc., and are subjected to prolonged loads at relatively high temperatures, with the effects of cyclic loading, temperature changes etc. [2, 6-8] also being relevant to their performance. Furthermore, while some studies have focused on unfilled rubbers, there are also many industrial usages which relate to filled rubbers, hence, the interest in composite materials based on rubber matrices in the literature [3, 4, 9, 10].

In contrast to most other types of materials, the mechanical behaviour of rubbers is far more complex. A major complication is caused by their large elastic strains. Their visco-elastic behaviour is also extensive, making it hard to differentiate between their time-dependent response rather than their ongoing viscous flow with a suitable formulation. Since rubbers normally contain a fairly low cross-link density, it might be expected that the actual viscous flow would be limited even in a long period of time. Beside this, if any creep-type behaviour is observed, then inelastic phenomena must be occurring and progressively developing with time. In terms of deformation micromechanisms, these could be rearrangement of molecular entanglement configurations, rupturing of cross-links or even breakage of backbone chain bonds.

Information about the basic mechanisms of creep in rubber is rather limited. It might be expected that creep resistance would be greater for rubbers with a higher cross-link density and indeed there are a few reports [11, 12] specifically confirming this.

The differences between true and nominal values of both stress and strain are sometimes ignored which has the potential to cause considerable confusion when analysing the behaviour of rubbers, since strains of rubbers tend to be large in contrast to other materials. Furthermore, both primary and secondary creep regimes are taken into account as with many creep situations. There is also a natural tendency for creep resistance to be reduced as the temperature is raised, although this is sometimes complicated by the associated increase in stiffness resulting from the entropy effect.

The effects of hard fillers might be expected to be somewhat simpler to predict than the basic response of the rubber, with a progressive increase in creep resistance expected when the filler content is raised. An explanation of this may be the consequence of load transfer from the matrix to the stiff reinforcement making the average stress level in the matrix lower and hence reducing the creep rate. On the other hand, the matrix stress state is commonly very inhomogeneous, with some regions being subjected to a higher local stress than that being applied [13]. In fact, there have been very few systematic studies of the effect of filler content on creep of rubber-based composites, with either particulate or fibrous reinforcement.

1.2 Research aims

This work is aimed at studying the creep behaviour of a particular (polyurethane) rubber, with and without particulate reinforcement, as a function of applied stress and temperature. Hence, there is a specific objective of obtaining basic information about the micromechanisms of creep deformation as well as establishing whether the dependence of the strain history on stress and temperature can be well captured by using an analytical expression, the Miller-Norton constitutive law, which is normally used for capturing the creep strains of metals. Further to this, short fibres, aligned along the loading direction, are expected to have a stronger effect on the creep behaviour of

reinforced composite rubber. Beyond these two scopes, it is also expected that an even stronger creep resistance might take place when the matrix material is replaced with a different type of rubber (silicone).

1.3 Thesis overview

Chapter 2 initially carries out a brief introduction about the structure and elastic deformation of rubber.

Chapter 3 introduces the concept of creep behaviour and the creep deformation for rubber.

Chapter 4 explains why uniaxial tensile test and uniaxial creep test are used as the experimental techniques for rubber and composite rubber, and describes testing procedures.

Chapter 5 particularly focuses on preparing the samples and running the tensile testing and creep testing for polyurethane (PU) rubber and the alumina particulate composite rubbers (polyurethane). The test results are presented at the end of the chapter.

Chapter 6 presents the sample preparation, tensile and creep testing and test results for the fibrous reinforced rubber (polyurethane).

Chapter 7 shows the sample preparation, tensile and creep testing and the test results for both the Polydimethylsiloxane (PDMS) rubber, commonly referred to as silicone rubber, and the fibrous reinforced variants (silicone).

Chapter 8 draws the conclusions and discusses the possible further work.

Chapter 2

Structure and Elastic Deformation of Rubber

Rubber (or elastomer) is one kind of polymer, and its properties are affected by cross-linking between the individual chain molecules. These cross-links are sufficient to prevent the unrestricted flow of whole molecules past nearby ones, but the chain segments between cross-links are free to move when the temperature is above the glass transition temperature, *Tg*. The segments of rubbers can uncoil and recoil. Thus, statistical theory is used to establish the mathematical relationships between the density of cross-links and material physical properties, for example, the stiffness. These relationships can be employed to predict the extension under a specific load, such as a balloon being inflated or a bungee jumper, or conversely, these measured properties can be used to calculate the extent of cross-linking.

There are more details about structure and elastic defamation of rubber which will be introduced in this Chapter.

2.1 Structure of Rubber

A rubber or elastomer is a fully amorphous, lightly cross-linked polymer, when it is above *Tg*. It is made up of many polymer molecules that contain many components of smaller repeated units termed monomers [14]. These polymer molecules are composed of a -C-C- backbone chain. Although the bond angle is fixed at 109.5°, in order to let the

macroscopic shape of the chain vary from being linear to coils and kinks, the torsion angle can change. As shown in Figure 2.1, blue line represents a C-C backbone chain in the left-hand side circle, and the end-to-end distance of the chain segment is indicated with the black arrow. Instead of aligning in a straight line, the chain segments always tend to coil up to some extent. This behaviour indicates that the system increases its entropy. The probability distribution of the end-to-end distance can be described mathematically.

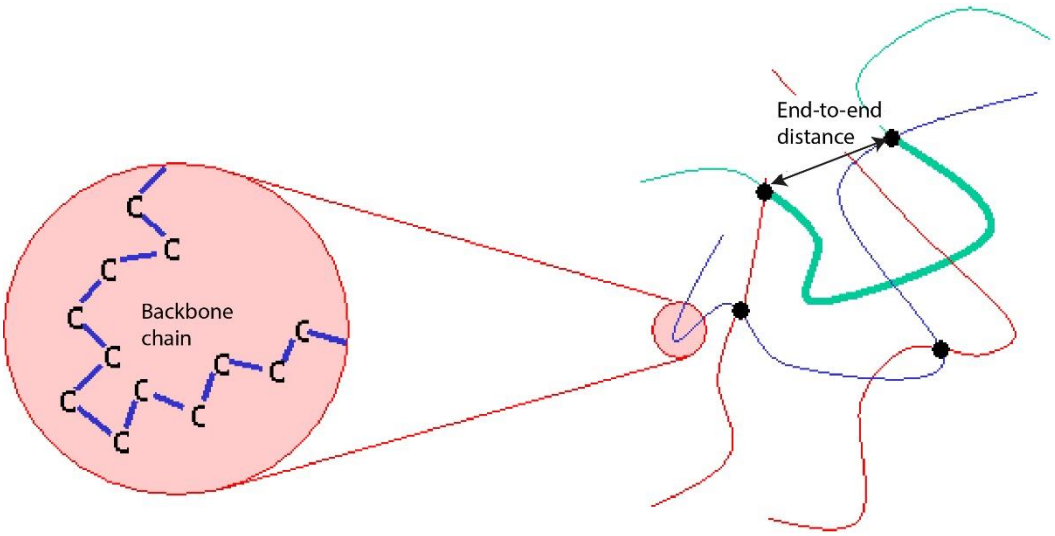

Figure 2.1: Structure of Rubber - form https://www.doitpoms.ac.uk/tlplib/stiffness-of-rubber/rubber-conformation.php

Since the molecules in rubber prefer to be coiled to a certain degree rather than stretched out, the polymer molecules easily get tangled together. As soon as chains become entangled, the mobility of rubber decreases, and it causes the stiffness of the rubber to increase.

Along with physical entanglements, the chains can connect to each other in another manner. If the chemical condition of the chain is suitable, an atom from one chain can form a chemical bond with an atom belonging to another chain. This bond is a type of a cross-link, which is covalent bond. The cross-links restrict the motion of the polymer chains and therefore raise the stiffness of the rubber.

2.2 Rubber Elasticity

When a rubber is placed under tensile loading, the polymer molecules in it will simultaneously change their relative disposition. Stretching a rubber and loading tension on its chains makes the polymers uncoil. These processes are shown schematically in Figure 2.2, in which a cross-linked structure of linear polymers can be shown by joining with other chains at black points along their length.

Figure 2.2(a) shows a conventional cross-linked rubber with chain segments coiled before loading with a tensile force. In Figure 2.2(b), the chain segments start to uncoil as far as they can before the cross-links reaches its limit. After that, the tension directly loads on the C-C bonds of the polymer backbone.

With continuing tension on the rubber, the extensibility of the chain segments reaches its limit. Finally all cross-links are broken and the chains make no inter-connection and the rubber is stretched into a very thin cross section leading to fracture.

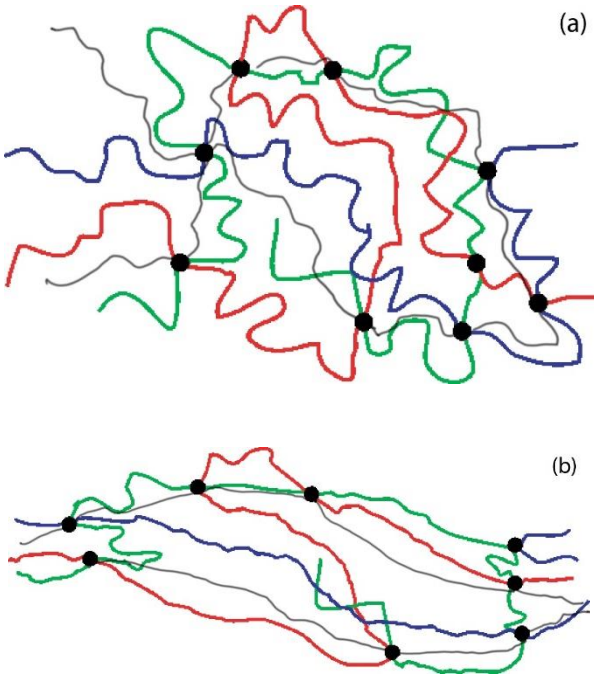

Figure 2.2: Stretching a rubber: (a) unloaded coiled chains, and (b) loaded in tension – from https://www.doitpoms.ac.uk/tlplib/stiffness-of-rubber/rubber-conformation.php.

Since the tension load pulls directly on the C-C bonds of the polymer backbone, and when the force becomes great enough, the C-C bonds will break, and the rubber will snap. The strength of the rubber is thus like other materials, although the stiffness is lower in magnitude. When extending rubber, the shape of the extension versus force graph is predictable.

It is common knowledge that most materials expand when heated. Fundamentally, the tendency for interatomic bond lengths to increase with rising temperature is for all materials due to the asymmetrical shape of the energy-spacing relationship (Lennard Jones Potential), which shows the increased average spacing between atoms or molecules in materials since they vibrate with greater amplitude at higher temperature. Rubber expands like other materials under normal conditions when it is heated. However, when under tension, it contracts in the loading direction, rather than elongates because the cross-linking mechanism is further activated by heating [15]. The explanation of this behaviour lies in the critical contribution of entropy to the elasticity of rubber. The stiffness of rubber is much lower than other materials because rubbers deform elastically by uncoiling of long convoluted molecules, rather than by stretching of individual inter-atomic bonds, thus decreasing internal entropy.

According to the classical (entropy-dominated) rubber elasticity theory, the equation that arises for the nominal stress during uniaxial tensile loading is usually written:

$$\sigma_N = kTn\left(\lambda - \frac{1}{\lambda^2}\right) \tag{2.1}$$

where k is the Boltzmann constant (1.38×10^{-23} J mol^{-1} K^{-1}), T is the absolute temperature, n is the number of chain segments per unit volume and λ is the extension ratio.

The extension ratio can be converted to the nominal strain of rubber:

$$\lambda = \frac{l}{l_0} = 1 + \varepsilon_N \tag{2.2}$$

where l_0 is the initial length of rubber, l is the extended length of rubber and ε_N is the nominal strain of rubber. Hence, Equation (2.1) can be re-expressed in terms of nominal strain,

$$\sigma_N = kTn\left(1 + \varepsilon_N - \frac{1}{(1+\varepsilon_N)^2}\right) \tag{2.3}$$

The relationships between true and nominal stresses and strains are shown as:

$$\sigma_T = \sigma_N(1+\varepsilon_N) \tag{2.4}$$

and

$$\begin{aligned} &\varepsilon_T = \ln(1+\varepsilon_N), \ ie \ \ e^{\varepsilon_T} = (1+\varepsilon_N) \\ &\therefore \varepsilon_N = e^{\varepsilon_T} - 1 \end{aligned} \tag{2.5}$$

where σ_T is the true stress and ε_T is the true strain of rubber.

Therefore, Equation (2.3) can be rewritten in terms of true stress and true strain.

$$\begin{aligned} &\frac{\sigma_T}{1+\varepsilon_N} = \frac{\sigma_T}{1+(e^{\varepsilon_T}-1)} = kTn\left(1+(e^{\varepsilon_T}-1) - \frac{1}{\left(1+e^{\varepsilon_T}-1\right)^2}\right) \\ &\therefore \sigma_T = e^{\varepsilon_T} kTn\left(e^{\varepsilon_T} - \frac{1}{\left(e^{\varepsilon_T}\right)^2}\right) = kTn\left(e^{2\varepsilon_T} - \frac{1}{e^{\varepsilon_T}}\right) \end{aligned} \tag{2.6}$$

This true stress σ_T is the applied (true) stress (in MPa) which is used in Equation (3.5) for the pure rubber creep test. Rubbers may be combined with particulates or stiffer filaments to form a composite. Therefore, there is another method to calculate the applied (true) stress for those filled rubbers.

2.3 The Eshelby Method for Particulate and Short Fibres

The effects of inert, hard fillers upon creep resistance of rubber composites might be easier to predict than the basic response of the rubber matrix alone with a progressive increase in creep resistance expected as the filler content is raised. An effect of this type is expected as a result of load transfer from the matrix to the stiff reinforcement, making the average stress level in the matrix lower and hence reducing the creep rate. On the other hand, at least with particulate reinforcement, the matrix stress state is actually very inhomogeneous, with some regions being subjected to a higher local stress than that being applied [13]. Also, the overall load transfer is not very effective with relatively low volume fractions of particulate reinforcement.

There have been very few systematic studies of the effect of filler content on creep of rubber-based composites. The potential complexities have been noticed when studying metal matrix composites (MMCs). While there are various reports [16, 17] of the steady state creep rate (at given temperature and stress) being reduced as the volume fraction of (particulate) reinforcement is raised, particle shape, interfacial bond strength, clustering of particles etc can all be significant [18]. Hard particles or short fibres can actually impair creep resistance in some cases [19, 20], particularly if measured in terms of creep rupture performance.

There are some other factors that could affect the creep of rubbers and rubber-based composite materials. For example, subsequent creep characteristics could be affected if extended periods at elevated temperature cause matrix ageing effects [21]. There has also been interest [2, 6, 8, 22] in mechanical and thermal cycling (ie fatigue-type effects). However, these studies have mainly been directed to specific industrial applications with only little focus on fundamentals.

The Eshelby method was originally outlined in 'thought experiments' by J.D.Eshelby [23, 24] in the late 1950s. The power and versatility of this approach soon became fully approved and a short time later various aspects of the concepts were brought together [25]. It continues to be employed for composite materials used in a wide range of

relevant mechanical applications [26-29]. Furthermore, it can also be used to model thermal and electrical conduction [30, 31].

His method involves calculation of the resultant stresses within the inclusion which is assumed to have an ellipsoidal shape. It is useful that many shapes can be approximated to ellipsoids. In particular for this work, a short fibre can be represented by a prolate ellipsoid with the same aspect ratio, which s = 1.

Eshelby originally focussed on an infinite matrix containing a (stiff) 'inclusion' (filler) with an ellipsoidal shape with the system initially stress-free. The inclusion is removed and undergoes a change of size and shape (a 'stress-free' strain). The inclusion is then subjected to surface forces in order to return to its original dimensions and replaced in the hole from where it came. The forces are removed, allowing the inclusion to adopt a new shape constrained by distorting the matrix. This is what happens on heating a matrix containing an inclusion, when the two have different coefficients of thermal expansion [13]. In addition, the original treatment addressed to an isolated inclusion in an infinite matrix, effectively a 'dilute' composite. The work from later researchers concerned the influence of other inclusions ('mean field' theories) to be taken into account, enabling macroscopic properties of real composites to be predicted.

Since the inclusion dimensions are significant in the Eshlby method, it is presented as one of the important parameters, aspect ratio, *s*, which is usually written as:

$$s = l / d \tag{2.7}$$

where *l* is the inclusion length, *d* is inclusion diameter.

From this equation, the aspect ratio for particulate must be one. For fibres, it is very diverse according to the varied fibre length. We only used particulate and short fibres in this study.

Other effective parameters are Young's modulus, E, and Poisson ratio, v, for both filler and matrix. These constants could be obtained either from direct measurement or material specification sheet, which came along with the raw material.

Hence, the stiffness tensor of the composite can be expressed below after some mathematical manipulation [13, 32]:

$$C_c = \left[C_m^{-1} - f\left\{ \left(C_f - C_m\right)\left[S - f\left(S - I\right)\right] + C_m \right\}^{-1} \left(C_f - C_m\right) C_m^{-1} \right]^{-1} \tag{2.8}$$

where C_m is the stiffness of matrix, C_f is the stiffness of filler, S, Eshelby tensor, a simple function which depends on aspect ratio (i.e., the aspect ratio of the filler) and the Poisson ratio of the matrix, f is the reinforcement volume, and I is the identity tensor.

The stiffness tensor, C_c, is a fourth rank tensor with 81 elements. Thus, it is best calculated in several computer programs (written in Pascal) for this work [32].

After the elastic deformation of rubber, creep will take place and lead to deformation. A discussion of creep behaviour is given in Chapter 3.

Chapter 3

Creep Deformation

When subjected to stress above the yield stress, σ_Y, materials deform plastically. By contrast, if the stress is lower than the yield stress, then it undergoes only instantaneous elastic deformation. However, it may deform permanently after extended periods under loading. This behaviour is usually termed creep. Creep tends to be sensitive to temperature, which affects the rates of diffusion. In general, creep starts to become significant when the homologous temperature (T/T_m) is greater than about 0.4 [33], although clearly, the stress level is also important.

3.1 Three Stages of Creep

Creep is often taken to comprise three stages, primary (transient creep), secondary (steady state) and tertiary (final) (see Figure 3.1), where strain is plotted as a function of time and applied stress. The steady-state creep is important for most of the component design because the other two stages are often brief compared with the secondary stage and they do not contribute much to the overall service life of a component. Deformation during primary creep is not well understood, with changes in microstructure often confusing the issue. Also, the elastic strain, which is a function of the temperature and stress applied to the material, will be recovered when the load is removed. The strain rate usually falls to a constant value after a certain time in secondary (steady-state) creep. During tertiary creep, flaws develop in the microstructure, typically voids

growing along grain boundaries. The strain rate accelerates with the accumulation of voids, and soon fracture occurs.

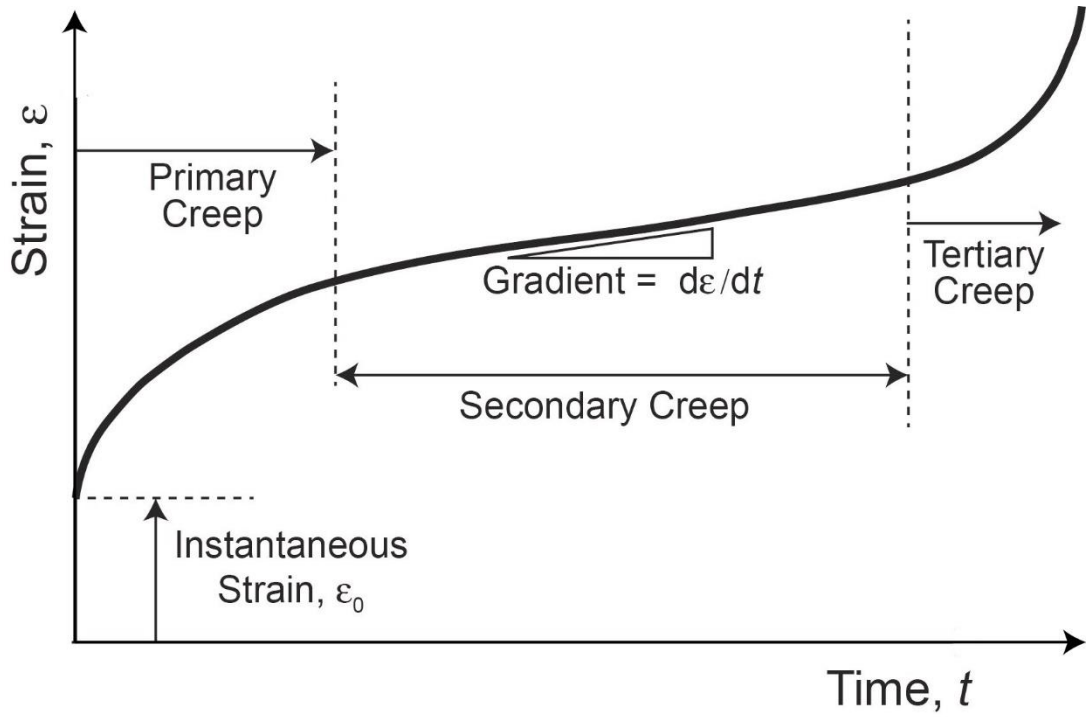

Figure 3.1: Three stages of creep deformation.

3.2 Conventional Creep Testing and Stress Relaxation Testing

Conventional creep testing is typically run by applying constant uniaxial (nominal) stress, which is lower than the yield stress. Force is applied axially to generate a uniform stress in the samples. Tests are run at a specific temperature with tensile or compressive loading.

Constant-loading equipment is typically employed to obtain creep data. The cross-section of the area of the specimen changes as a function with time. However, since the creep strains are relatively small, the changes in effective stress can be neglected.

A set of creep curves obtained from uniaxial tensile creep tests in which the strain varies as a function of time with four applied stresses ($\sigma_1 > \sigma_2 > \sigma_3 > \sigma_4$), is shown in

Figure 3.2. These tests can be run from a few hours to a several thousand hours, depending on the material, stress or temperature.

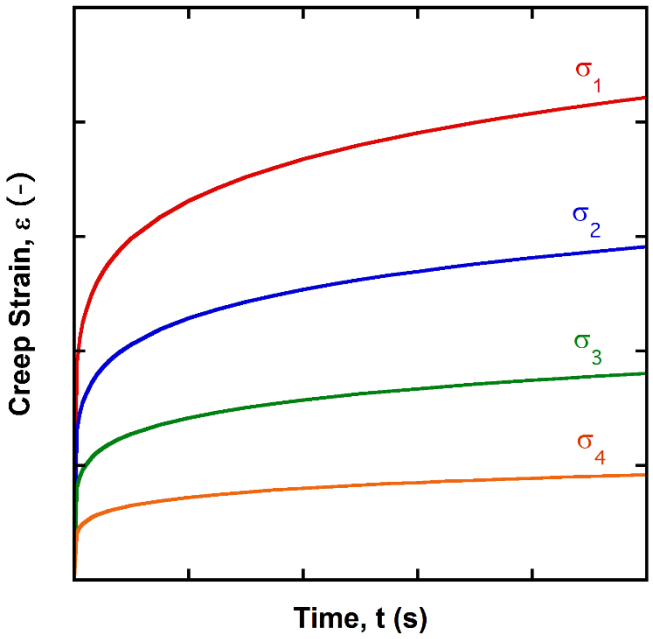

Figure 3.2: Creep curves increase with time, for four different stress levels.

The stress - relaxation test is another method to evaluate the material stress as a function of time. Creep causes stresses to relax in a material under constant displacement at a specific temperature for a period [33]. This method should not be confused with constant load creep test method, in which constant stress is employed. They are both creep tests.

Since the relaxation relieves the stress, it takes place with a function of time at various stress levels. A set of relaxation curves is shown in Figure 3.3.

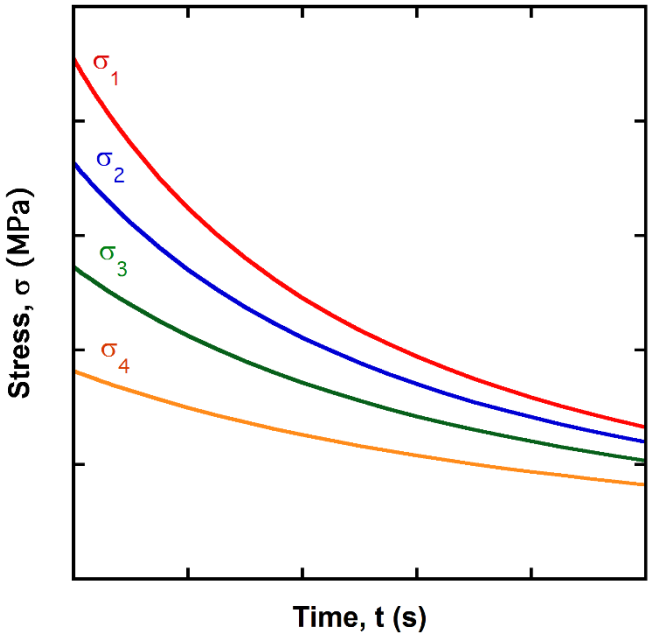

Figure 3.3: Stress relaxation curves decrease with time.

This type of test is generally less popular than constant stress creep test due to the need to vary the load during the test.

3.3 Effects of Stress and Temperature on Creep Rate

The strain rate reaches a constant value, which is determined by stress and temperature during the secondary (steady-state) stage. Normally, this is the region that shows the greatest interest during creep deformation since it lasts for long periods of time and generates large creep stains. The equation governing the strain rate of steady state creep is:

$$\dot{\varepsilon}_s = A\sigma^n \exp(-Q/RT) \tag{3.1}$$

where Q is activation energy, n is stress exponent, A is constant, R is the universal gas constant, and T is the temperature in Kelvin.

Thus;

$$\ln \dot{\varepsilon}_s = \ln A + n \ln \sigma - Q/RT \tag{3.2}$$

The stress exponent n can be determined by plotting the $\ln \dot{\varepsilon}_s$ against the $\ln \sigma$, as shown in Figure 3.4. It indicates that the variation of creep mechanisms is dominated by different stresses. The lower stress regime shows a value $n \sim 1$, while the high-stress regime shows $n > 3$ [34].

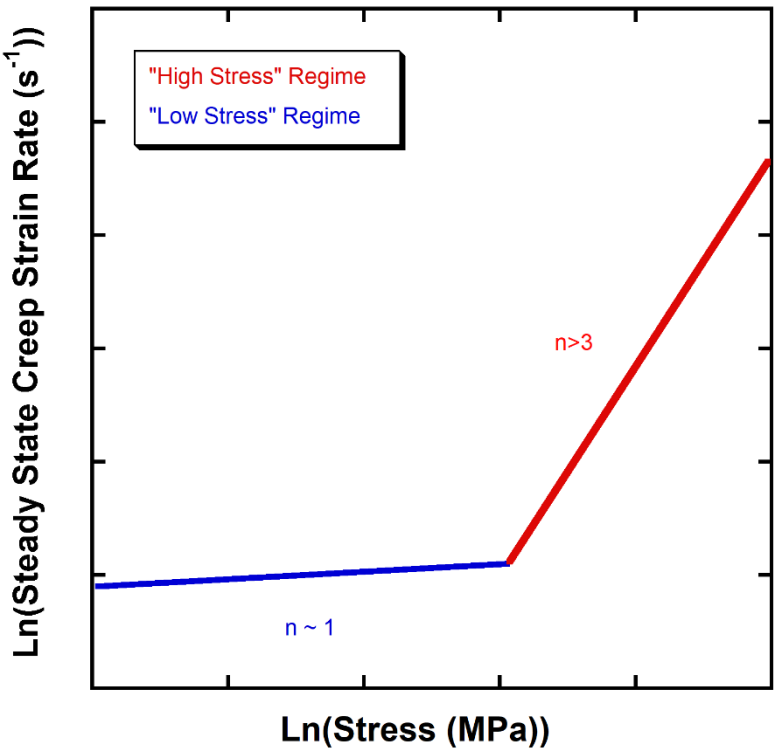

Figure 3.4: Variation stress with the calculation of creep exponent, n.

The activation energy Q can be determined experimentally with plotting the $\ln \dot{\varepsilon}_s$ of creep rate against the $1/T$ (see Figure 3.5). It shows that the creep rate increases exponentially with temperature. The activation energy is approximately equal to the lattice self-diffusion, Q_{SD}, at high temperature, and grain boundary diffusion, Q_{GB}, at low temperature [34].

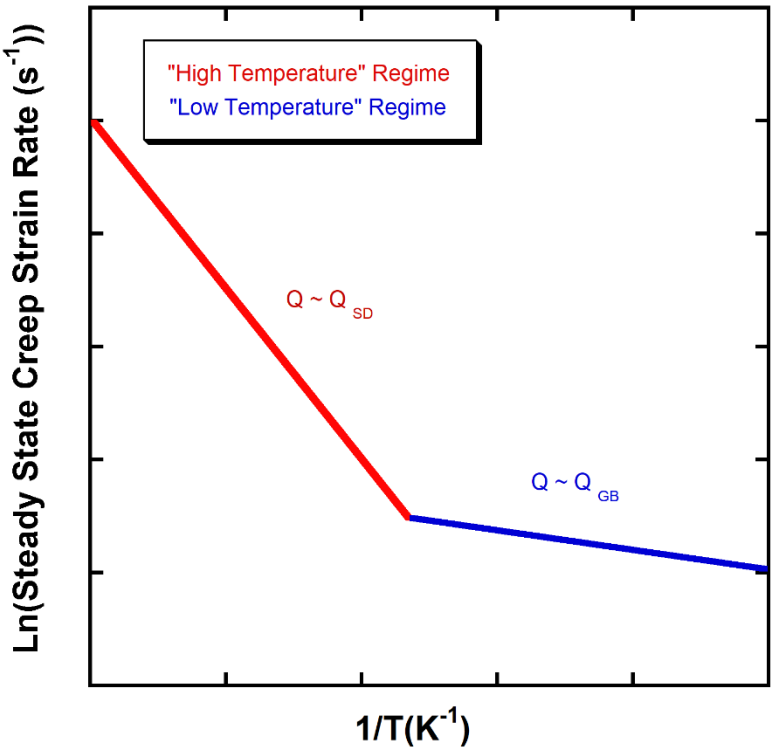

Figure 3.5: Variation of creep rate with temperature.

3.4 Conventional Viscoelastic Material Fitting Method

In relaxation test, the material is forced to a sudden strain that is kept constant during the test and the stress of material monitored continuously. The initial stress is affected by the elastic response of the material; therefore, the stress relaxation will take place. To take viscoelasticity into account, a suitable mathematical model should add the time effect to the model. The most popular mathematical model of this behaviour is Prony series as [35]:

$$g_g(t) = 1 - \sum_{i=1}^{N} g_i (1 - e^{-t/\tau_i}) \tag{3.3}$$

where g_i is a material constant and τ_i is the relaxation time. g_g is the dimensionless shear relaxation modulus, which can be defined as:

$$g_g(t) = \frac{G(t)}{G_0} \tag{3.4}$$

where $G(t)$ and G_0 are the time dependent and the initial shear moduli, respectively. This method was also introduced to extract the model parameters of rubber-like materials [36].

However, as we know that a creep test is usually easier to operate than a relaxation test, most data are available as creep compliance against time. Unfortunately, no relationship has been developed for expressing creep compliance in terms of the coefficient of the Prony series. So, if one has creep data, it is not easy to get the coefficients of the relaxation (Prony series) and vice versa. Park, et al [37] presented a method of interconversion between relaxation modulus and creep compliance for linear viscoelastic materials. Furthermore, Loy, et al. [38] also proposed various algorithms to solve the interconversion equation for linear viscoelasticity when Prony series are given for the relaxation and creep moduli.

Unfortunately, no easy way to convert between relaxation modulus and creep compliance data for general viscoelastic materials has been found, even by using a commercial FEM software. To bring in an effective way to capture the creep behaviour of these rubbers and rubber composite materials, a new constitutive law will be discussed in the following section.

3.5 Creep Constitutive Law Used in This Work

There are several ways that attempt to characterise the creep behaviour of pure rubbers. The term “creep of rubbers” must be used with caution. “Creep” is normally recognised when the material is progressively straining under constant stress, (or in many practical cases, constant load), while “stress relaxation” means the progressive reduction in stress applied to the sample when it is constrained with a constant strain. When analysing these situations, variations between true and nominal values of both stress and strain are sometimes ignored, which can potentially cause considerable confusion since strains of rubber tend to be large. The assumption might be established that both types of tests offer the same deformation mechanisms involvements, thus the relationships found to apply for these two should be linked. Regarding on this, Oman

and Negode [4] showed how stress relaxation behaviour of filled rubbers could be captured using measured creep characteristics, while taking into account the progressively decreasing stress level. This, however, required a creep relationship that considered both primary and secondary creep. An example of such a relationship is the expression commonly termed the Miller-Norton constitutive law [39-41], which may be written:

$$\varepsilon_{cr} = \frac{C\sigma_T^n t^{m+1}}{m+1} = \frac{A\sigma_T^n t^{m+1}}{m+1} \exp\left(\frac{-Q}{RT}\right) \tag{3.5}$$

in which ε_{cr} is the (true) creep strain, C and A are both constants (units of $MPa^{-n}\ s^{-(m+1)}$), t is the time (s), σ_T is the applied (true) stress (in MPa), n is the stress exponent, T is the absolute temperature, R is the universal gas constant and m is a dimensionless constant that controls the shape of the time dependence. This form of the equation is based on the assumption that the creep is a thermally activated process, with an activation energy of Q in k J mol^{-1}.

There is limited information available concerning the basic creep characteristics of rubbers. It might be expected that creep resistance would be greater for rubbers with a higher cross-link density and indeed there are a few reports [11, 12] specifically confirming this. There is also a natural tendency for creep resistance to be reduced as the temperature is raised, although this is sometimes complicated by the associated increase in stiffness (dominated by the entropy effect). It is perhaps worth noting that there have not only been very few specific studies of the effect of temperatures, but also, they usually cover only a relatively narrow temperature range.

Kartsovnik [42] proposed that viscous flow of rubbers, in which the resistance to flow increases as the applied stress is raised, is described in terms of an activation energy for the flow that progressively rises with increasing stress. His treatment considered the dominance of the entropy term during elastic deformation of rubbers and incorporated the large differences between nominal and true stress and strain values during deformation of rubbers. However, a model in which the activation energy is variable

leaves a considerable degree of freedom when evaluating parameter values and is thus rather difficult to verify. Kartsovnik subsequently [43] developed this further, offering a capability for prediction of creep rates from a knowledge of the elastic behaviour, again using viscosity concepts and underlying physical models incorporating various combinations of springs and dashpots. Promising levels of agreement were reported, although they did require specific calibration factors in each case. Of course, as with other types of material and mechanical response, virtually any constitutive law is simply an empirical relationship containing arbitrarily adjustable parameters, and checking for fit is essentially a curve-fitting operation. Nevertheless, the Kartsovnik model is certainly not an easy one to apply or use for predictive purposes although it does recognize the significance of the large elastic strain in rubbers. Hence, Equation (3.5) has been used for this work.

As σ_T is the applied (true) stress (in MPa) in Equation (3.5), it is converted from the nominal stress in Equation (2.4).

The experimental technique for testing the tension and creep behaviour of rubber will be described in next Chapter.

Chapter 4

Experimental Technique

Creep tests may involve stressing specimens in almost any mode, e.g. tension, compression, flexure, shear, etc., depending on the material application. A few comprehensive tests that combine the above stress modes may be useful to address the creep behaviour of rubbers. For example, according to the ISO (International Standard) 7743 [44], compression stress - strain properties of rubber can be measured by using its compression test. However, compressive creep testing is not feasible for rubbers because the barrelling caused by the friction needs to be optimised [45] during the elastic deformation. Therefore, the uniaxial tension creep test is the most widely employed since it is simple to set-up and effectively carry out [46].

The elastic deformation of rubber takes place before creeping, and thus the cross-section of the specimen with a corresponding constant load needs to be defined in a tensile test.

4.1 Tensile Test Technique

A method used for the determination of the tensile stress-strain properties of vulcanized and thermoplastic rubbers is introduced in ISO 37 [47].

In this work, a Tinius Olsen H25KS universal tester, with a 250 N load cell, was employed for the tensile test. The set-up is shown in Figure 4.1(a). Displacements were

measured on the cross-head, using a system that monitored rotations of the lead-screws. This was considered acceptable in view of the very high compliance of the loading train, relative to that of the samples. Samples and gauge length were set differently depending on the materials and manufacturing process.

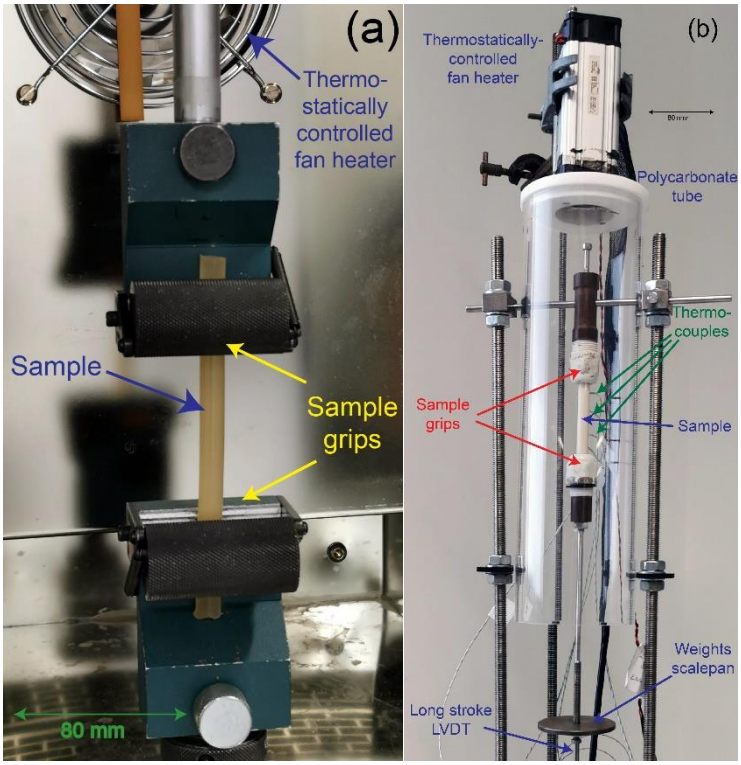

Figure 4.1: Photos of the set-up for tensile testing of: (a) stress-strain relationships and (b) creep characteristics.

A constant and relatively high displacement rate was set so that these tests were not too long. However, despite these short durations, it is possible that some creep could have occurred during them, since initial (primary) creep rates are quite high in these materials, particularly at the higher temperatures. It is also important to note the (relatively large) differences between nominal and true stresses and strains during elastic deformation (of rubber).

4.2 Creep Test Technique

Creep tests were carried out by applying a constant load to the test specimen and measuring its displacement as a function of time.

According to the general guidance in ASTM 2990 [48], the creep testing of rubbers, the specimen alignment is critical. Also, the load direction deviation should be within 1% of the axis of specimen loading, the extensometer for the measurement of change in length should be sensitive, and the tests should be all performed at a constant temperature. Creep tests were run with the customized set-up shown in Figure 4.1(b). The grips were radially symmetric, which helped reduce the danger of slippage. Figure 4.2 (a) illustrates both head and tail of the sample were griped with two sample holders. Figure 4.2 (b) shows that the sample holder was modified from a hose conneter with a black rubber seal ('O' ring) inside. When the white cap was screwed down, the sample could be held with a strong clamping force that came from the collet and the black rubber seal.

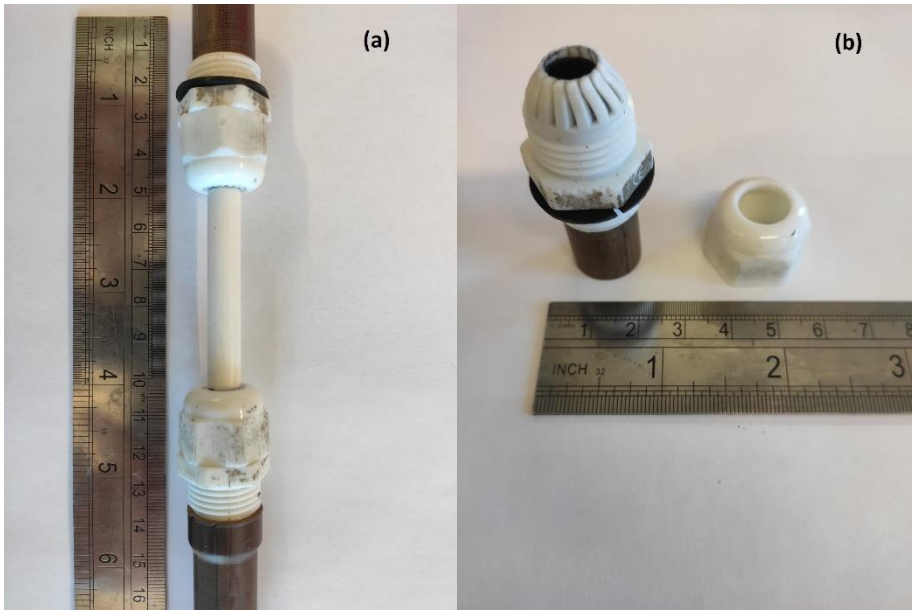

Figure 4.2: Illustration of the sample grips for tensile creep test: (a) a sample with both grip holders (b) disassembling one of the grip holders.

Displacements were measured using a long travel linear variable differential transformer (LVDT). The procedure adopted was that the system was first equilibrated thermally by switching on the heater, while temperature was governed by three thermocouples in contact with the sample on top, middle, and bottom. This was done with the sample under a small load – just the weight of the scale-pan. The system had relatively small thermal inertia, so the time for equilibrium to be reached was relatively short - typically about 5-10 minutes. This can be seen in the thermocouple output plots shown in Figure 4.3 and Figure 4.4, in which it is also clear that the variations in temperature along the length of the sample were relatively small.

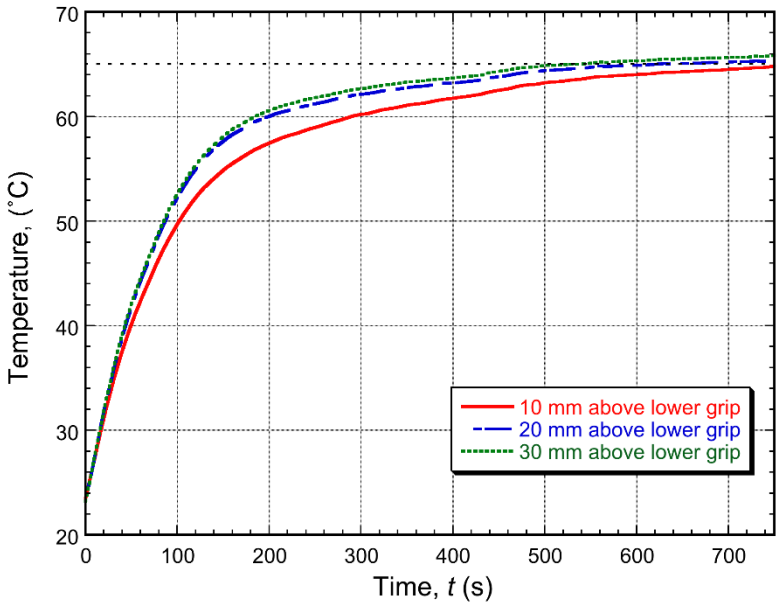

Figure 4.3: Outputs of the thermocouples in contact with a pure polyurethane rubber sample during the initial heating period (before the start of a creep test to be carried out at 65°C).

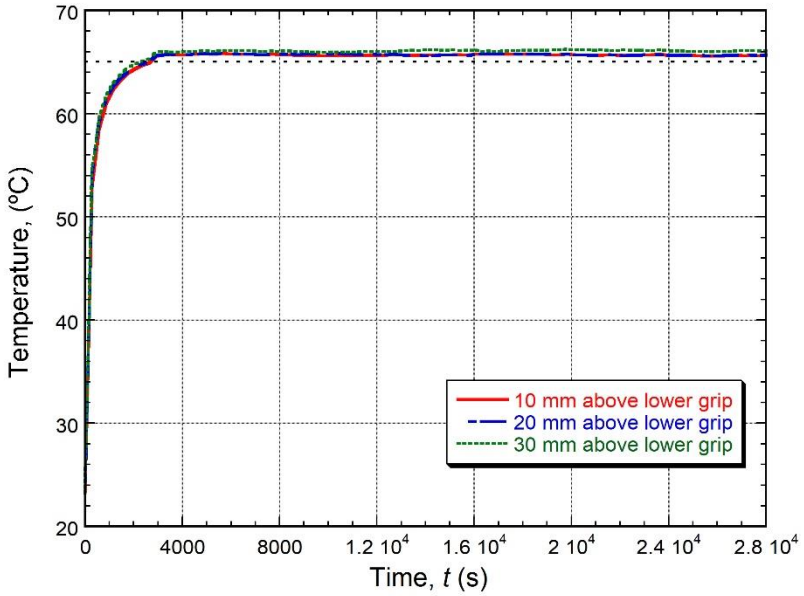

Figure 4.4: Outputs of the thermocouples in contact with a pure polyurethane rubber sample for about 8 hours (2.8 x 10^4 seconds) at 65°C.

Once the sample and environment had reached thermal equilibrium, the load concerned was quickly applied to the scale pan. Furthermore, a short period followed during which the system reached some kind of mechanical equilibrium, which probably involved a degree of settling and load redistribution in the gripping system and loading train, as well as some oscillation. The extension measured during this period of mechanical equilibration (typically a few tens of seconds) was not primarily arising from actual creep of the sample, therefore, it was neglected when calculating the creep strain.

4.3 The Experimental Procedure

A summary of the experimental procedure is as follows:

i) A tensile test is employed to determine the stress-strain properties of rubbers. Both stress and strain were converted from nominal to true values by using Equation (2.4) and (2.5). Since the strains are positive in tensile, the true stress has a higher magnitude than the nominal value, while the true strain has a lower magnitude than the nominal strain and a plot of σ_T vs ε_T is produced.

ii) A uniaxial creep test is carried out with the constant applied load and it produces a plot of experimental creep strain vs time. The creep strain in the early stage (tens of seconds) needs to be discounted since the system needs to settle down after loading the constant load. The creep strain is measured as a function of time, i.e., σ, the true stress, and the time t are varied. Therefore, according to the Equation (3.5), ε_{cr}, is the true creep strain and σ is equal to the applied true stress, σ_T. For the composite rubbers, σ_T needs to be calculated by using a computer program based on the Eshelby model, which Clyne et al. [32] gave the details of coding in Appendix IV of their book. Since these programs were only working in Macintosh system, they have been translated into the codes that worked with Windows system for this work. A plot of predicted ε_{cr} vs. t can be produced after a comprehensive calculation.

It is worth noting that in all the above, it is assumed that a constant applied load gives rise to stress, σ. But the above procedures are valid only if the true stress corresponding to the reduction in the cross-section of the specimen after the elastic deformation is used.

Using the experimental techniques described, the following Chapter 5, 6 and 7 give more experimental details and results obtained from the different rubbers and rubber composites tested.

Chapter 5

Creep of Particulate PU Rubber

The work presented here is the creep response of a polyurethane (PU) rubber, with and without particulate reinforcement, as a function of applied stress and temperature.

5.1 Experimental Procedures

5.1.1 Polyurethane rubber - Poly 74-30

Polyurethanes (PUs) are versatile materials capable of use in different applications, typically based on their structure-property relationships. Modification of the raw materials and production procedures though proper methods could tailor the PUs for even wider and varied specific applications [49]. Polyurethane synthesis was created by linking the urethane groups (-NH-(C=O)-O-) into the molecular units [50]. In general, PUs are often synthesized from the reaction between an isocyanate and polymolecule with either a catalyst or ultraviolet light activation [51].

The special interest in polyurethanes is due to their crosslinking ability, chain flexibility and intermolecular force. Chains and cross-linking play important roles in PUs. Stretchy polymers contain long chains with low cross-linking, whereas hard polymers get shorter chains with high cross-linking. The cross-linking in PUs often give a very high molecular weight with a three-dimensional (3D) network build-up. A small number of PUs may be referred to as a “giant molecule” and this structure enables them not to go soft or melt when they are heated. Furthermore, soft polyurethane rubbers

offer great abrasion resistance, solvent and oil resistance, high tensile and tear properties, good resistance to ozone and oxygen, and good mechanical properties at low temperature [52].

In this work, a two-part polyurethane rubber (Poly 74-30, supplied by WP Northcott), was used: one part (A) being a Polyurethane monomer (with ≤ 1% toluene di-isocyanate – $CH_3C_6H_3(NCO)_2$) and the other (B) being Polyol and Di-ethyl-toluenedismine, $C_{11}H_{18}N_2$, which is an excellent long chain extender for PU. After mixing, they were cured at room temperature to flexible, high strength, mould rubbers. Due to the cross-linking, Poly 74-30 rubber is suitable for durable, easy-releasing moulds for casting plasters and waxes without release agents.

5.1.2 Sample Preparation

Three materials were used in the present work, all based on a 2-parts polyurethane (PU) rubber. These two liquid parts were warmed up to 50°C (to ensure good fluidity and remove air bubbles), mixed in equal weight ratios (1:1), and stirred for about a minute. A 20 ml syringe was employed to extract the mixture and extrude it into the mould [53], which was a polymeric straw with external diameter 9 mm and internal diameter 8.5 mm, see Figure 5.1. Once the straw was filled up, two rubber plugs with diameter in 8.5 mm were used to seal both ends. The sample was left at ambient temperature for about 16 hours for first stage curing, removed from the mould, and then put into an oven at 50 ˚C for 24 hours to complete the curing process.

Figure 5.1: Syringe, straw mould, and unfilled rubber sample.

For producing the filled (particle-reinforced) rubbers, the above procedure was modified slightly. Alumina powders (supplied by Plasmalloy) with an average particle size of about 30 μm, were blended with the Part B liquid at ambient temperature before the heating and mixing of the two liquids. The weight of powder added was such as to give 10 vol% or 20 vol% of particulates in the final product. The rest of the procedure was the same as that for the unfilled rubber. These mixtures were slightly less fluid with the presence of particulate, but it was still possible to extract it with the syringe and inject it to fill the mould.

5.1.3 Microstructural Characterisation

Polyurethane rubber was used as matrix for both composite materials in this work. The microstructure of the two composite materials was examined with Scanning Electron Microscopy (SEM) on sections that were produced by using a microtome. The SEM Back-Scattered Electron (BSE) micrographs in Figure 5.2 demonstrate both that the spatial distribution of the (alumina) reinforcement particles is fairly uniform and that the interfacial bonding appears to be good. (Some damage inevitably arises during sample preparation by the cutting, but the matrix does appear to have “wetted” the particles quite well. A little porosity can be observed in the matrix, possibly slightly

more in the material with the higher filler content, although it appears in both cases to be relatively low.

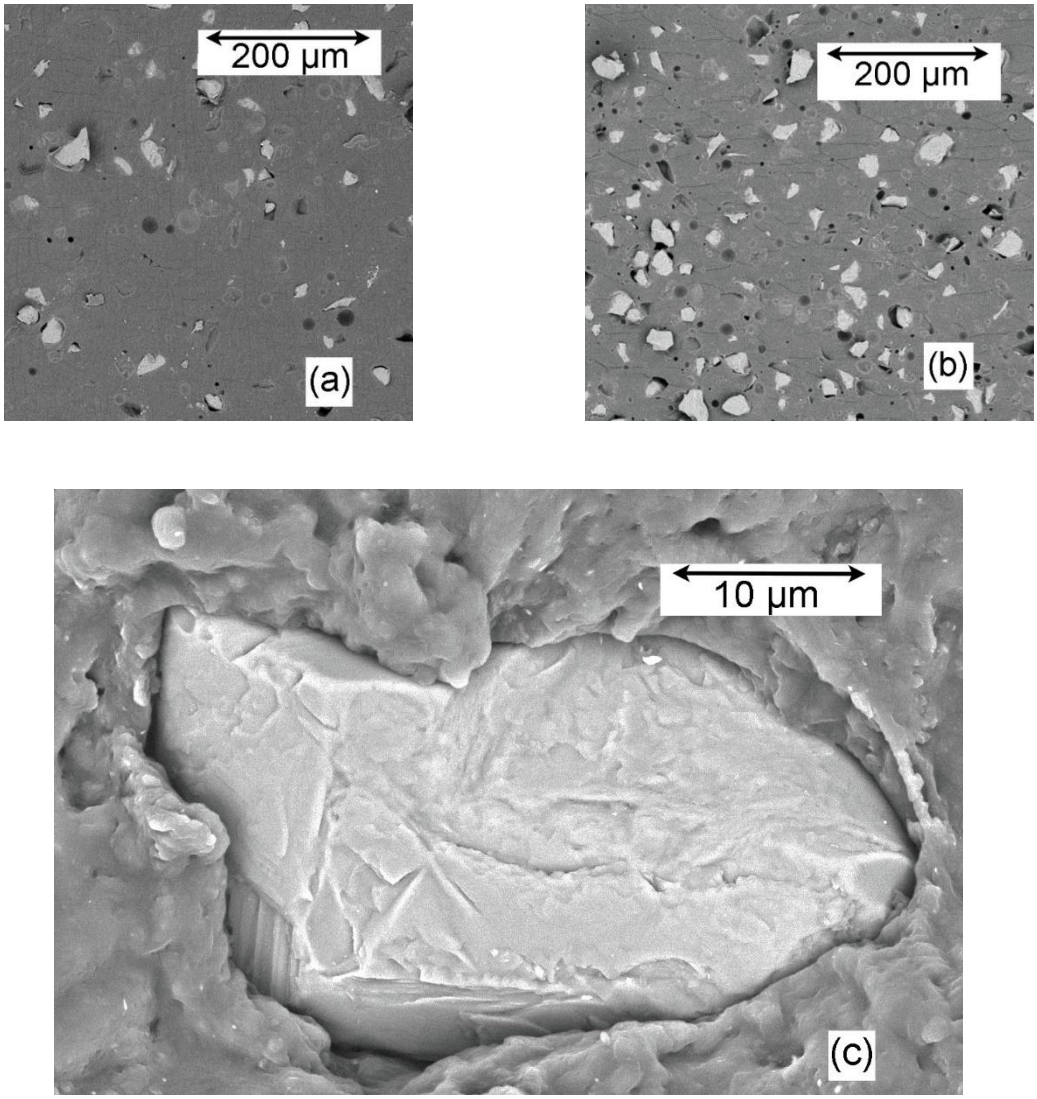

Figure 5.2: SEM image of polished sections from composite containing: (a) 10 vol% Al_2O_3, (b) 20 vol% Al_2O_3, and (c) 20 vol% Al_2O_3 at higher magnification.

In order to explore this a little further, and to obtain information about the actual volume fractions of reinforcement, density measurements were carried out for all three materials. This was done by using two techniques - simple weighing of the samples (with their volume obtained from measured diameter and length) and hydrostatic weighing,

using deionized water as the immersion fluid (with a density of 0.987 g cm^{-3} at 20°C). The outcomes are shown in Table 5.1, where the average measured values were 1.015, 1.29 and 1.60 g cm^{-3} for these three materials, with very similar values being obtained using the two techniques. The density value quoted by the supplier of the rubber is 1.006 g cm^{-3}. This is very close to the measured value, suggesting that the porosity levels in the unfilled rubber were low (<1%). It is possible that the levels were slightly higher in the composite materials, although their densities are very close to the values expected in the absence of porosity and with the planned volume fractions of reinforcement (taken to have a density of 3.99 g cm^{-3} [13]). It therefore seems likely that all three materials were effectively free of porosity and contained the planned levels of reinforcement.

Material	**Densities (g cm^{-3})**				Standard Errors
	Direct Measured	Hydrostatic Measured	Average Measured	Expected	
Unfilled rubber	1.01	1.02	1.015	1.006	0.0031
10 vol% Al_2O_3 composites	1.28	1.30	1.29	1.299	0.0047
20 vol% Al_2O_3 composites	1.61	1.59	1.60	1.588	0.0051
Al_2O_3				3.99	

Table 5.1: Densitometry data for the three materials.

5.1.4 Mechanical Testing

Two tests were carried out, in each case on all three materials and at three temperatures (20°C, 45°C and 65°C). These were, firstly, the conventional tensile stress-

strain curve measurement, which was taken in the elastic regime, and then, secondly, tensile creep testing.

5.1.4.1 Tensile Testing

The tensile testing set-up is shown in Chapter 4. Samples were about 90-100 mm long in total, with a gauge length of about 75 mm.

A constant displacement rate of 1.67 mm s^{-1} was used, which was corresponding to an approximate strain rate of 0.02 s^{-1}. This was a relatively high rate and the test lasted only about 30 s.

Both stress and strain levels were converted from nominal to true values by using Equation (2.4) and (2.5). Since the strains are positive in tension, the true stress has a higher magnitude than the nominal value, while the true strain has a lower magnitude than the nominal strain.

5.1.4.2 Creep Testing

Creep tests were carried out with the customized set-up that is described in the Chapter 4.

Three types of materials, which were the unfilled PU rubber and the two particulate composites, were used in this uniaxial tensile creep test. Once the sample and environment had reached thermal equilibrium, which took about 5 to 10 minutes, the load was quickly set on the scale pan. Three loads were used in the current work, which were 9.8 N, 11.8 N and 14.7 N. This loading quickly generated (relatively large) elastic extension. Moreover, a short period allowed the system to reach mechanical equilibrium, which may involve a degree of settling and load redistribution in the gripping system, loading train, and some oscillation. Therefore, the extension measured in the mechanical equilibration period (a few tens of seconds) was discounted when plotting the creep strain.

5.2 Experimental Results

5.2.1 Tensile Testing Results

Figure 5.3 shows the stress-strain plots obtained, which show: (a) nominal and (b) true values. Plotted as true stress and strain, these materials are quite close to being linearly elastic. A single Young's modulus value can thus be ascribed to them, as shown in Figure 5.3(b). Some sensitivity to temperature can be observed, which may be at least partially due to some minor creep effects. However, this dependence isn't significant.

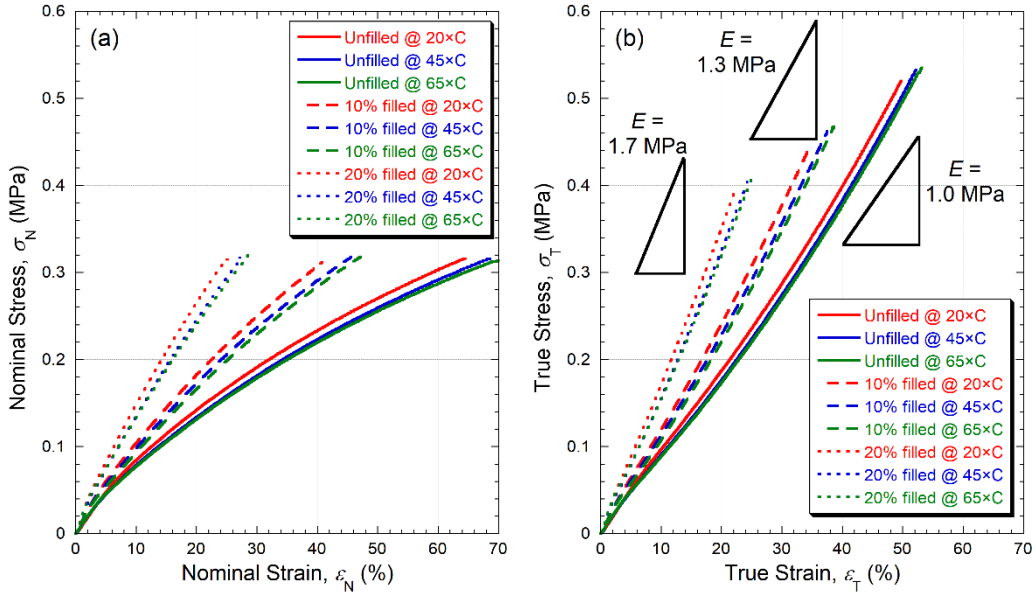

Figure 5.3: Stress-strain data from tensile tests on the 3 materials at 3 different temperatures, plotted as (a) nominal and (b) true values.

According to the Expression (2.3), Figure 5.4 presents a comparison between the experimental curve for the unfilled rubber and plots of this equation for three different values of n at 20°C (T = 293 K). It is clear that a fairly good agreement is obtained for $n \sim 6.5 \times 10^{25} m^{-3}$. It is difficult to make an accurate independent measurement of n, but this value is certainly in the range expected.

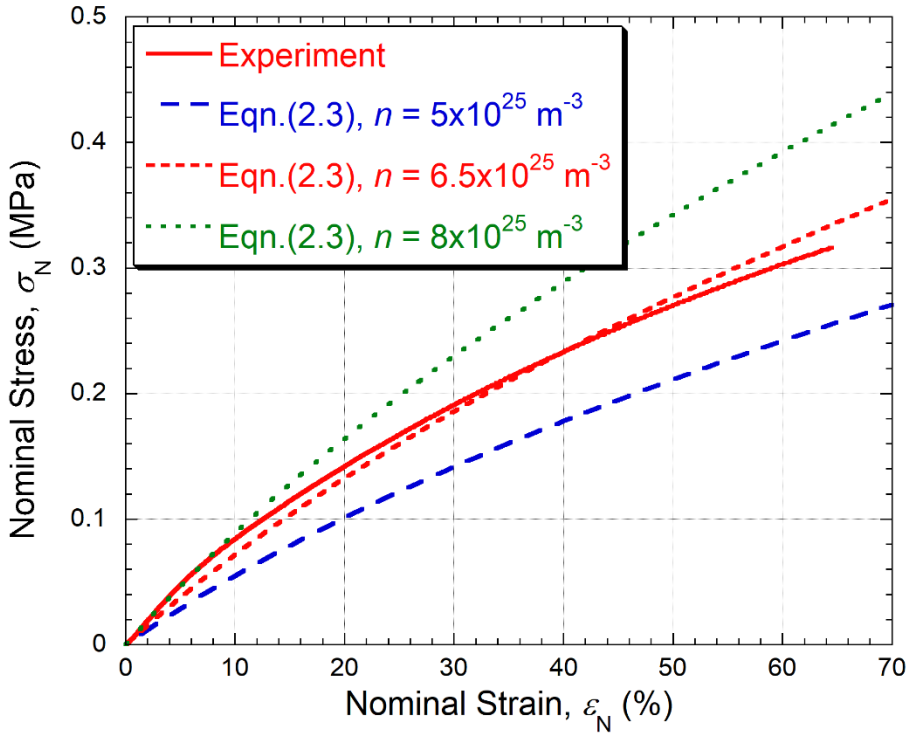

Figure 5.4: Comparison between the experimental nominal stress – strain curve for the unfilled rubber at room temperature and predictions from the classical equation (Equation 2.3) from rubber elasticity theory (entropy-dominated), with three different values for the number of chain segments per unit volume (related to the cross-link density).

The stiffening produced by particulate additions is broadly consistent with composite theory. For example, Figure 5.5(a) shows that it is approximately as predicted by using the Eshelby model, based on spherical reinforcement. The elastic constants used in the model are shown in Table 5.2. and inputted in a computer program based on Expression (2.8). The increase in *E* due to 20% of particles is relatively small, despite the huge filler/matrix *E* ratio. This is because the load transfer to (stiff) spheres is quite limited at these addition levels. (If the same volume fraction of aligned fibres had been added, with this reinforcement/matrix *E* ratio, then the increase in composite stiffness in the alignment direction would have been much greater.) This limited load transfer is quantified in Figure 5.5(b), which shows that, with 20% of spheres, the average matrix stress is still about 85% of the applied stress.

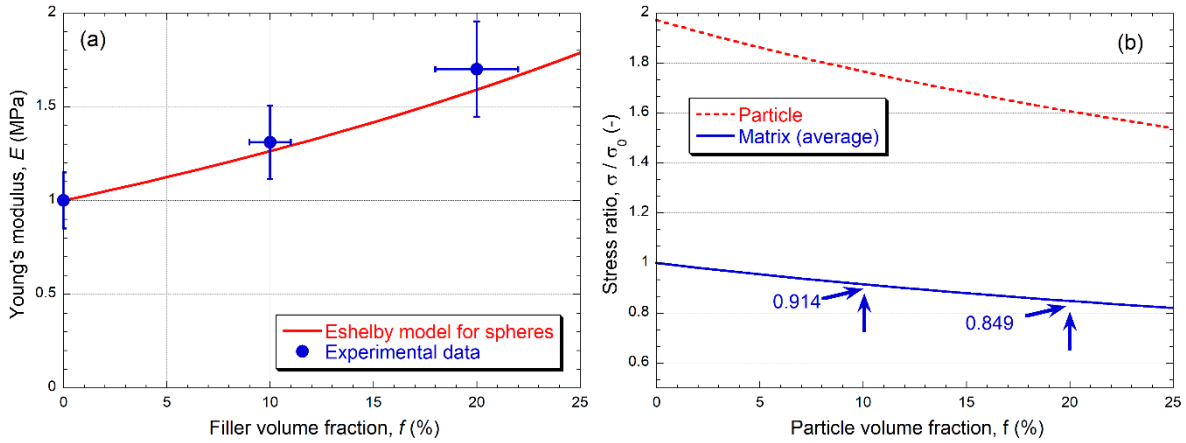

Figure 5.5: Eshelby model predictions for alumina spheres in a rubber matrix, as a function of reinforcement volume fraction, showing (a) Young's modulus (with measured values) and (b) ratio of the stress in the two constituents to the applied stress.

Material	Young's modulus, *E*(GPa)	Poisson ration, *v* (-)
Rubber	0.001	0.48
Al_2O_3	300	0.22

Table 5.2: Elastic constants were employed in the Eshelby modelling.

5.2.2 Creep Testing Results

As previously mentioned, a formulation that captures both primary and secondary regimes of creep strain histories, with a smooth transition between them, is that of Miller-Norton (Equation (3.5)). Obtaining the best-fit set of parameter values for a particular experimental creep curve is simply a mathematical exercise, preferably carried out using a convergence algorithm in parameter space. In the present work, this was done using a Nelder-Mead treatment [54, 55], in a form that was fully described [56] (for a target outcome of the shape of a residual indent). It should again be noted that both the strain being monitored, and the stress level used in the formulation are true values. The stress level was taken as the true value at the start of the creep (after the elastic deformation). This was obtained from the applied load by converting it to a nominal stress using the original sectional area of the samples and then using Equation (2.4) and (2.5), knowing the nominal elastic strain (obtained from the plots in

Figure 5.3(a)). The further (small) changes in true stress as the creep progressed were neglected.

5.2.2.1 *Creep Characteristics of the Unfilled Rubber*

A comparison is shown in Figure 5.6 between measured creep strain histories (at 20°C) and best-fit Miller-Norton curves, for three different applied loads. The experimental strain values correspond to measured extensions (after elastic deformation) divided by the elastically strained length (to give an effective nominal strain) and then converted to a true strain using Equation (2.5).

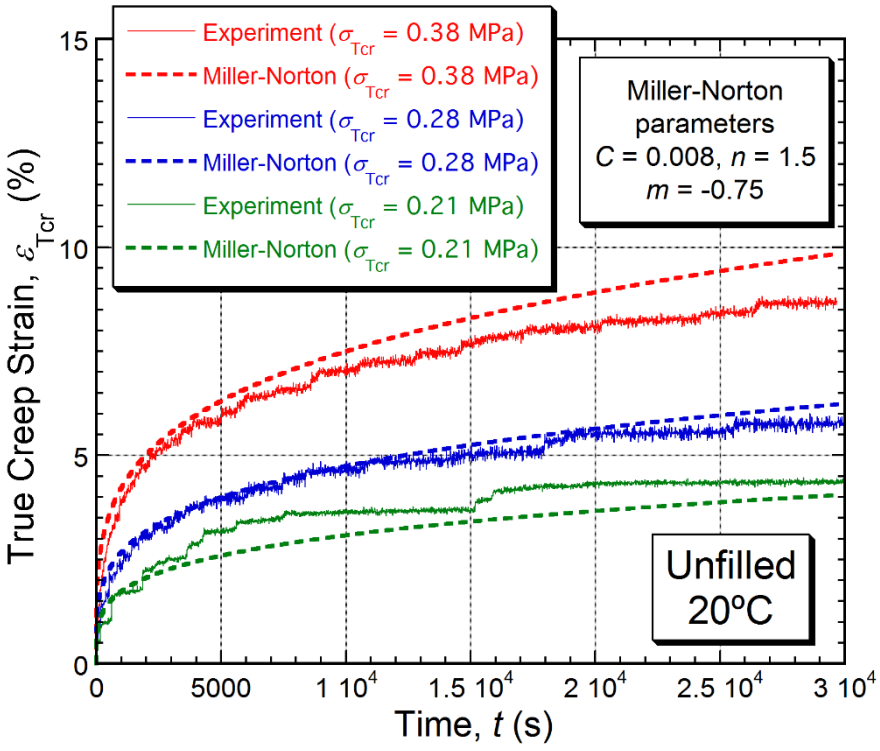

Figure 5.6: Comparison between measured and modelled creep strain histories for the unfilled rubber at 20°C, with the true stress at the start of the test (after elastic deformation) having the values shown in the legend.

It can be seen that, in general, the creep characteristics can be captured quite well using the Miller-Norton model, for the 3 different levels of applied stress. There is some evidence of the straining not always being entirely smooth and progressive, for which there could be several possible explanations, for example, under the same loading, the

displacement of rubber or composite rubber normally is larger than the metal or other higher density materials, but in general the data appear to be systematic. It was confirmed that, on removal of the load, the elastic component of the total strain was immediately recovered, but the creep strain was permanent (apart from a small amount of visco-elastic recovery). Since each creep test only took about 8 hours in this work, the permanent strain was insignificant and could be neglected.

From the form of the Miller-Norton equation (Equation (3.5)), the only effect of changing the temperature is to alter the value of *C*, with its dependence on temperature providing a means of estimating the activation energy for the creep process. Corresponding plots to that of Figure 5.6, for temperatures of 45°C and 65°C, are shown in Figure 5.7(a) and (b), with only the value of *C* being used to optimize the fit and the values of *m* and *n* being maintained at those found to be appropriate for the 20°C curves. While the fit is naturally not perfect, it does appear that the behaviour is being broadly captured using this formulation.

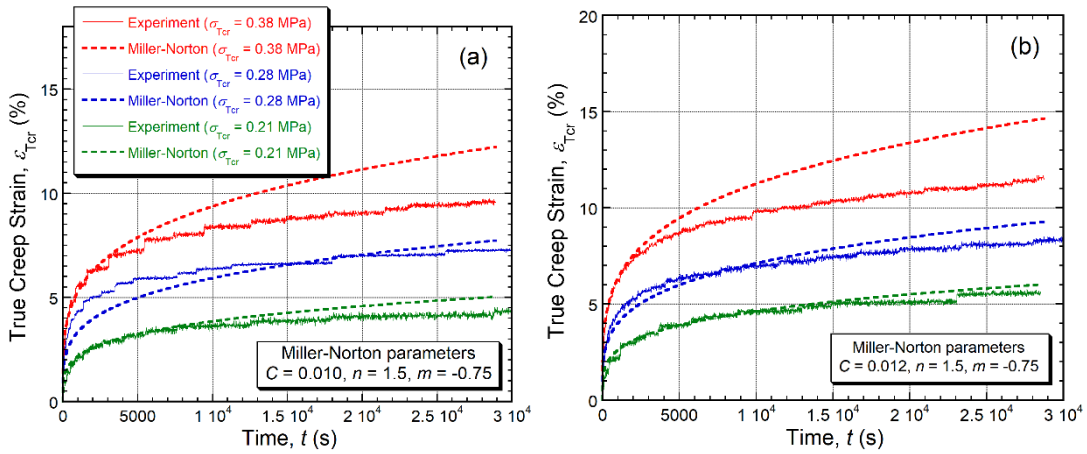

Figure 5.7: Comparison between measured and modelled creep strain histories for the unfilled rubber at (a) 45°C and (b) 65°C. The true stress values at the start (after elastic deformation) are shown in the legend of Figure 5.7(a).

This dependence of the value of *C* on temperature can be used to estimate the activation energy, *Q*, for the creep process, assuming that it has the Boltzmann dependence of Equation (3.5). The Arrhenius plot shown in Figure 5.8 indicates that the

value is about 7.4 kJ mol $^{-1}$. Of course, the data on which this is based are very limited, but this value is probably a meaningful estimate. It is relatively low, but that is expected for a polymeric material of this type, in which the rate-determining process is probably some kind of (untangling) rearrangement of the chain structure.

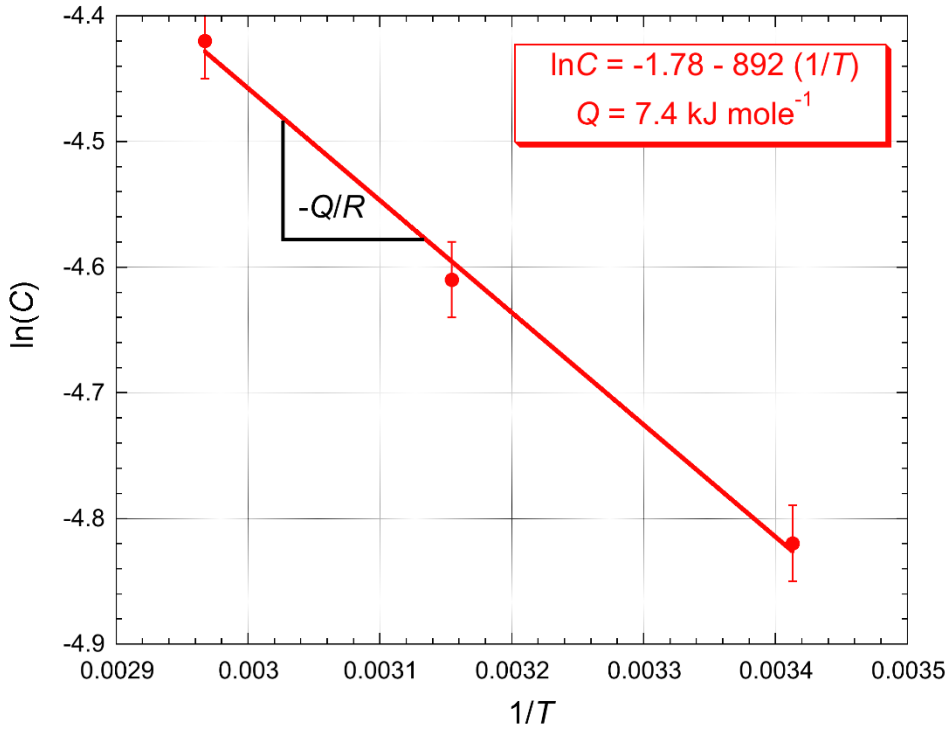

Figure 5.8: Arrhenius plot of the three C values, with an estimate of the activation energy Q being obtained from the gradient.

5.2.2.2 Creep Characteristics of the Rubber Composites

There is also interest in how the creep characteristics are modified by the presence of stiff particulates, which in effect will not deform at all during the testing. It should first be noted that, while the same applied loads were used for all 3 materials, the greater stiffness of the composites meant that the elastic strains were lower and so the true stresses were also lower. This effect will reduce the creep rate, even if the actual creep resistance of the material is no greater. One way to see whether the creep resistance is

in fact any greater is to use the same Miller-Norton parameter values as for the unfilled rubber and check whether the experimental curves fall below them.

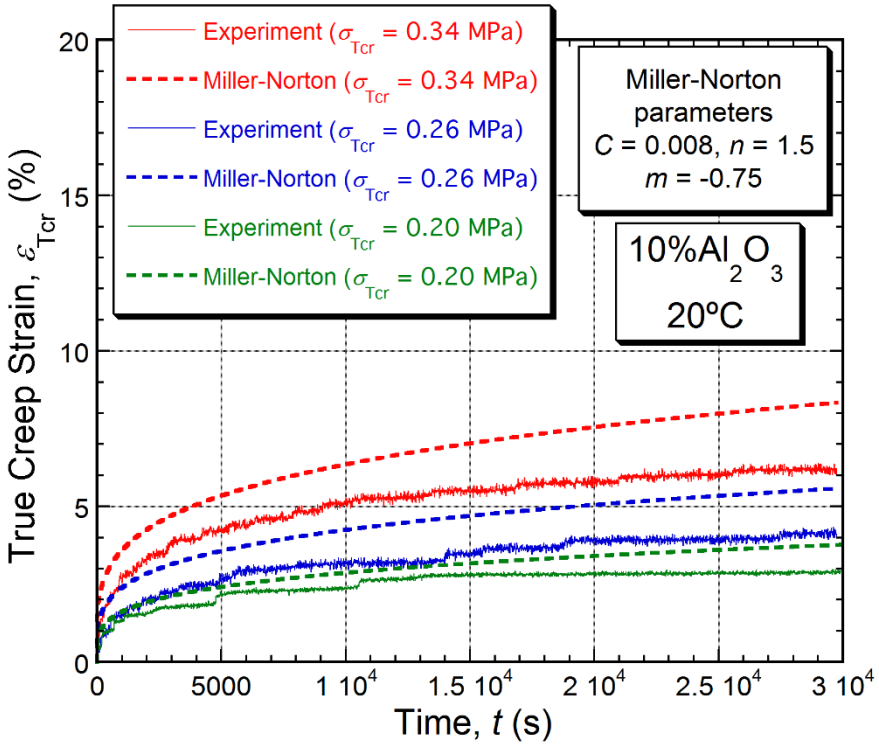

Figure 5.9: Comparison between measured and modelled creep strain histories for the 10% filled rubber at 20°C, with the true stress at the start of the test (after elastic deformation) having the values shown in the legend.

The outcome of this operation, for each of the temperatures, is shown in Figures 5.9 and 5.10 for the 10% filled composite. It can be seen that the experimental plots are consistently below the Miller-Norton predictive curves, showing that the material exhibits superior creep resistance to the unfilled rubber, beyond what would be expected on the basis of its higher stiffness. This is consistent with the expected load transfer to the particles (and also with the concept of the particles remaining well-bonded to the matrix). On the other hand, the improvement is not a dramatic one, which might have been expected from the limited nature of the load transfer (and indeed of the stiffening effect).

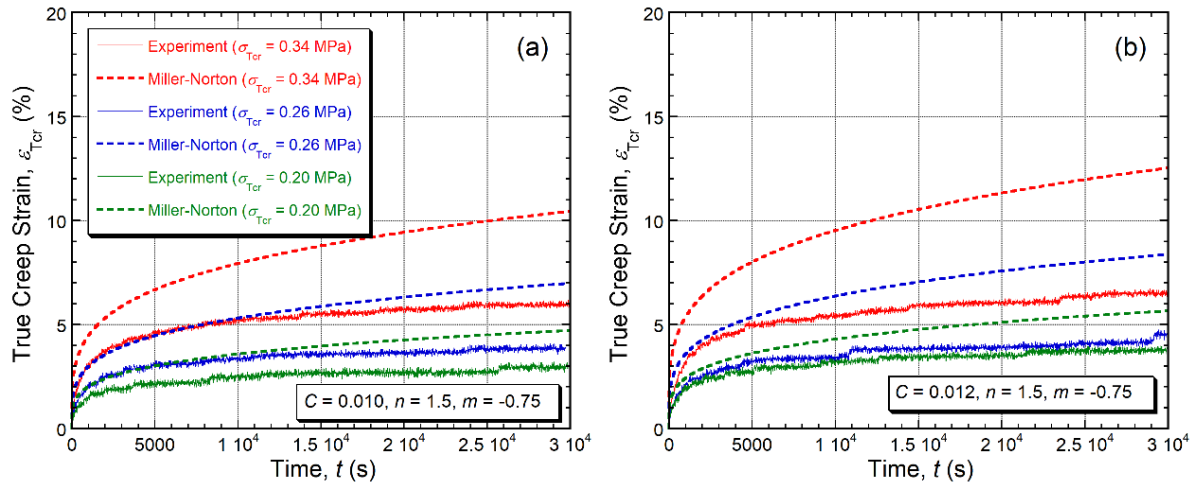

Figure 5.10: Comparison between measured and modelled creep strain histories for the 10% filled rubber at (a) 45°C and (b) 65°C. The true stress values at the start (after elastic deformation) are shown in the legend of Figure 5.10(a)

Corresponding plots for the 20% filled composite are shown in Figures 5.11 and 5.12. This also shows consistent outcomes, with the experimental plots further below those corresponding to the unfilled rubber, with account taken of the effect of the higher stiffness. Moreover, the differences are significantly greater than for the 10% composite, consistent with the creep resistance being further enhanced by the increased filler content.

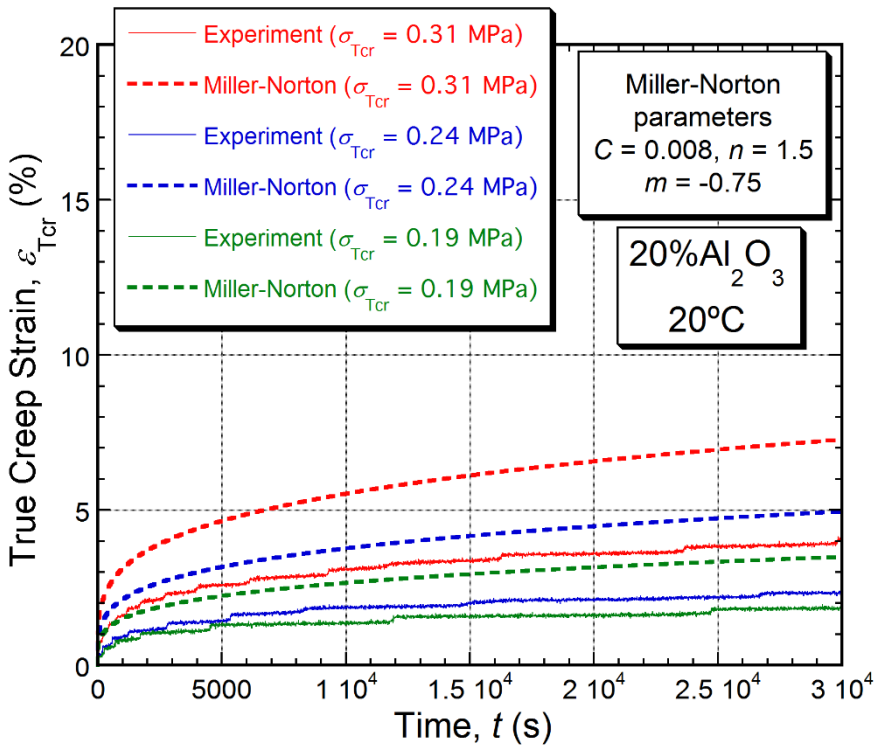

Figure 5.11: Comparison between measured and modelled creep strain histories for the 20% filled rubber at 20°C, with the true stress at the start of the test (after elastic defamation) having the values shown in the legend.

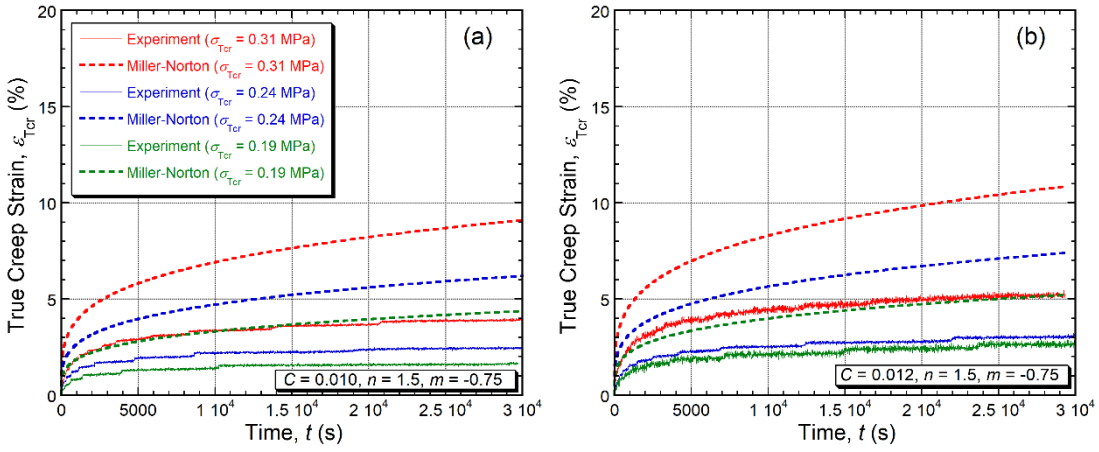

Figure 5.12: Comparison between measured and modelled creep strain histories for the 20% filled rubber at (a) 45°C and (b) 65°C. The true stress values at the start (after elastic deformation) are shown in the legend of Figure 5.12(a).

The observed reductions in creep rate, due to the presence of the reinforcement, should be consistent with the behaviour expected based on the reduction in the average

stress in the matrix (as predicted in Figure 5.5(b)). The two plots in Figure 5.13(a) and (b) show, for the two reinforcement levels at 20°C, the effect of reducing the stress level in the Miller-Norton model by the factors concerned (0.914 and 0.849respectively). The resultant curves have also been multiplied by factors of 0.9 and 0.8 respectively, to reflect the fact that the volume of the sample in which the creep is taking place has also been reduced.

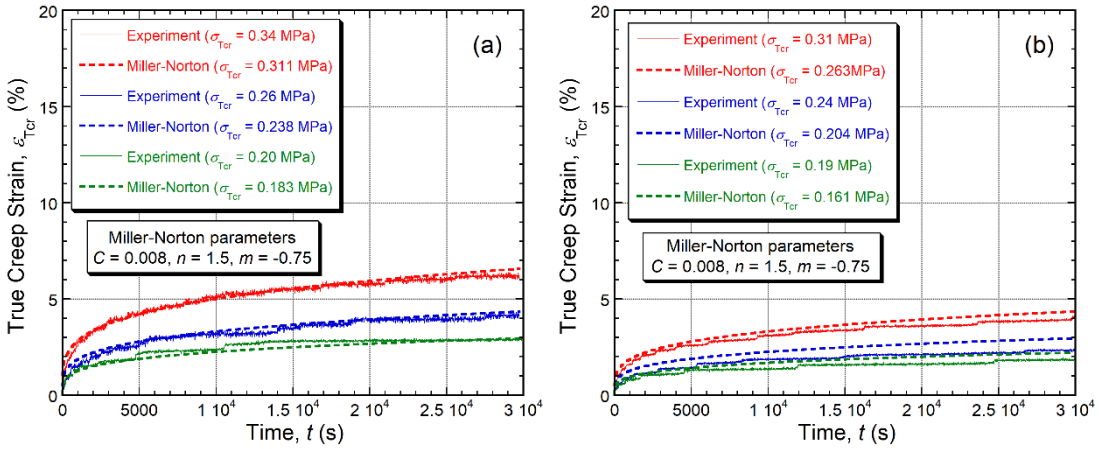

Figure 5.13: Measured and modelled creep strain histories at 20°C, for (a) 10% AL_2O_3 and (b) 20% Al_2O_3 composites. These modelled curves take account of the reductions in the mean matrix stress due to the presence of the filler and also the fact that the creep is taking place in a reduced volume fraction of the sample.

The agreement between experiment and model is good. Similar levels of agreement are obtained when the same operation is carried out for the two other temperatures. It is therefore clear that the creep behaviour of these composites can be predicted with a good level of confidence on the basis of stress transfer, using average matrix stress levels, despite the fact that, in particulate composites of this type, the local stress in the matrix varies quite strongly from point to point.

The load transfer from matrix to reinforcement is considerably greater (in the direction of alignment) when (short) fibres are used, and there is also less point-to-point variation in the matrix stress level. Next chapter is aimed at exploring the effects observed in rubbers of this type with fibrous reinforcement.

Chapter 6

Creep of Fibre - Reinforced PU Rubber

The work presented here concerns the creep of a particular PU rubber, with and without fibrous reinforcement, as a function of applied stress and temperature. The previous chapter reported on the effect of particulate reinforcement, which has a significant effect on reducing creep rates. However, this effect is not dramatic, which is attributed to the relatively low degree of load transfer from matrix to particles. Short fibres, aligned along the loading direction, are expected to have a stronger effect and the current chapter is focused on this issue.

6.1 Experimental Procedures

6.1.1 Material and Sample Preparation

Fibrous composites were produced using "Saffil" alumina fibres, supplied by Saffil Ltd (Widnes) loose in large bags. Their diameter is ~3 μm. Detailed information about this type of fibre, which has been extensively used as reinforcement for MMCs, is available in the literature [57-60]. In the as-received form, these fibres have lengths in the mm range, with the associated high aspect ratios creating extensive tangles - making the product an aggregated mass or "blanket". In order to convert this material into a form suitable for production of (aligned) composite material containing dispersed short fibres, a ball milling operation was carried out, using a DECO All-Direction Planetary Ball Mill. Four layers of fibre mats (5 g in weight each) were placed in a 1.5 litre alumina

chamber, interspersed with five layers of alumina balls (40 pieces each), of diameter 10.75 mm, see Figure 6.1. The rotation speed of the container was 300 rpm, with the direction of rotation reversed once per minute.

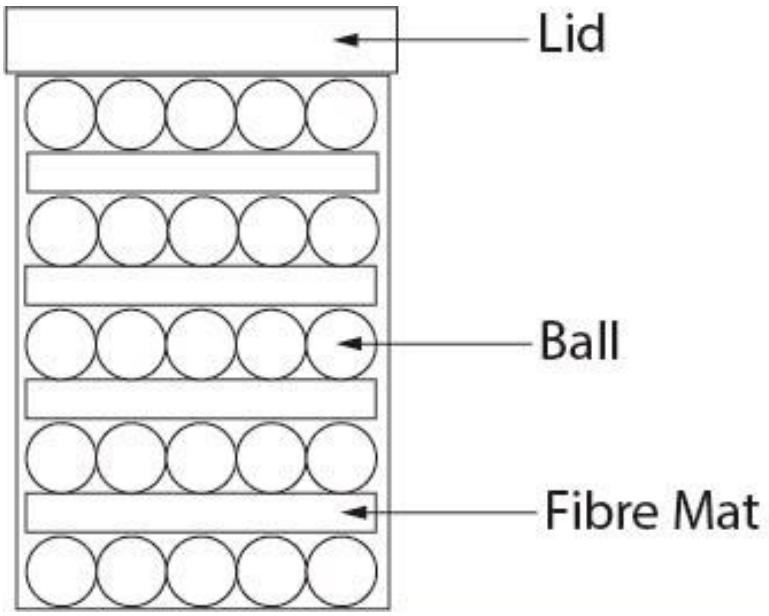

Figure 6.1: Ball Mill setting.

This ball milling operation disentangled the fibres and reduced the average fibre lengths to the range of a few tens of microns. The milling time was used as a variable to produce fibres with two different average aspect ratios. It was found that periods of 3 minutes and 7 minutes were suitable for this purpose. Figure 6.2 shows SEM micrographs of the resultant products. It can be seen that, in both cases, the product contained a range of fibre aspect ratios, but there is clearly a difference between the two, with the shorter period (Figure 6.2(a)) leading a value apparently of the order of 10-30 and the longer period (Figure 6.2(b)) to something like 5-15. However, issues concerned with sampling and possible further changes or selectivity during production of the composite are such that it is not really useful to attempt to measure an average aspect ratio from images such as these. Theoretically, the alignment of fibres should be in the axial (loading) direction in the matrix. However, in practice, the orientation of the fibres in the matrix is based on extrusion process, viscosity of the matrix material and the length of the short fibre – in other words, it is few chance to axially align all

short fibres in the matrix [32]. Thus, the average measured aspect ratio of short fibres cannot be valid. Instead of that, an estimated value based on the aspect ratio of particulate(s = 1) may be more effective.

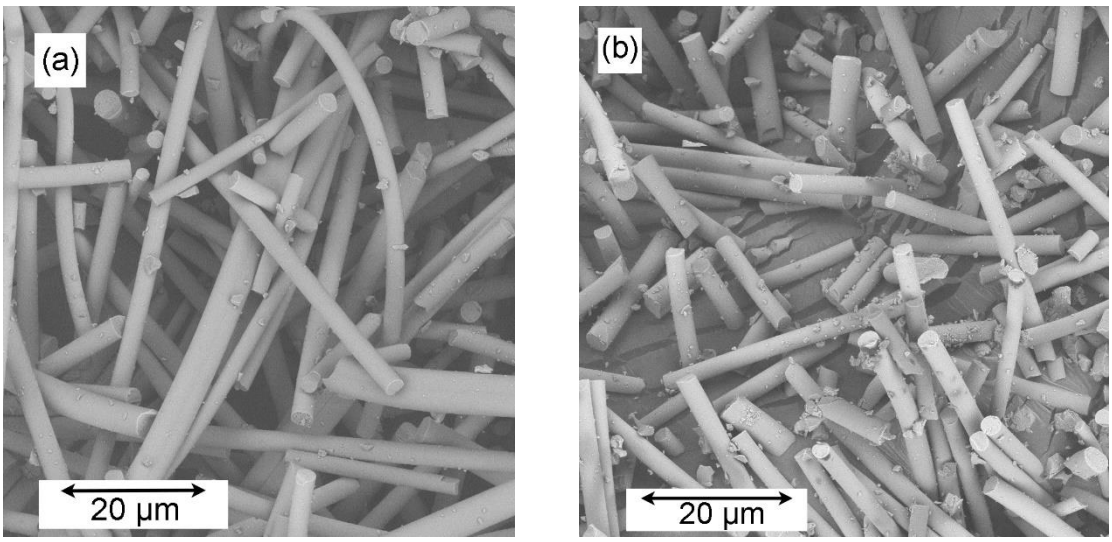

Figure 6.2: SEM images of Alumina fibres after milling periods of: (a) 3 minutes and (b) 7 minutes.

As the previous Chapter presented, PU rubber is based on a 2-part (Poly 74-30, supplied by WP Northcott), one part (A) being a Polyurethane monomer (with $\leqslant$ 1% toluene di-isocyanate) and the other (B) being Polyol and Di-ethyl-toluenedismine. The alumina particulate was equiaxed, with a particle size around 30 µm. Fibre-reinforced composites were manufactured using a similar (blending and extrusion) technique (see Chapter 5), producing cylindrical samples of 8.5 mm diameter. However, while particulate composites were successfully manufactured with reinforcement contents of 10% and 20% (by volume), fibre contents above 10% created mixtures with a too high viscosity for extrusion. Fibre composites were therefore made with target contents of 5% and 10% (by volume). These were produced using either the higher aspect ratio short fibres (3 mins. milling) or those with the lower range (7 mins. milling).

6.1.2 Microstructure Characterisation

It was shown in Chapter 5 that the spatial distribution of the reinforcement particles was fairly uniform and that the interfacial bonding appeared to be good. For the fibrous reinforcement, there is the additional issue of fibre alignment. The extrusion procedure does tend to produce alignment of the fibres along the axis of the sample, although this alignment is naturally not perfect. An impression of this, and also of the spatial distribution, can be obtained from Figure 6.3, which shows SEM micrographs of the four types of fibre composite. These shows both a “cut” (lateral) surface and a “fracture” (transverse) surface. While neither the degree of alignment nor the spatial uniformity is perfect, the fibres appear to be fairly well-dispersed and there is certainly a degree of alignment. It can also be seen that there is some porosity.

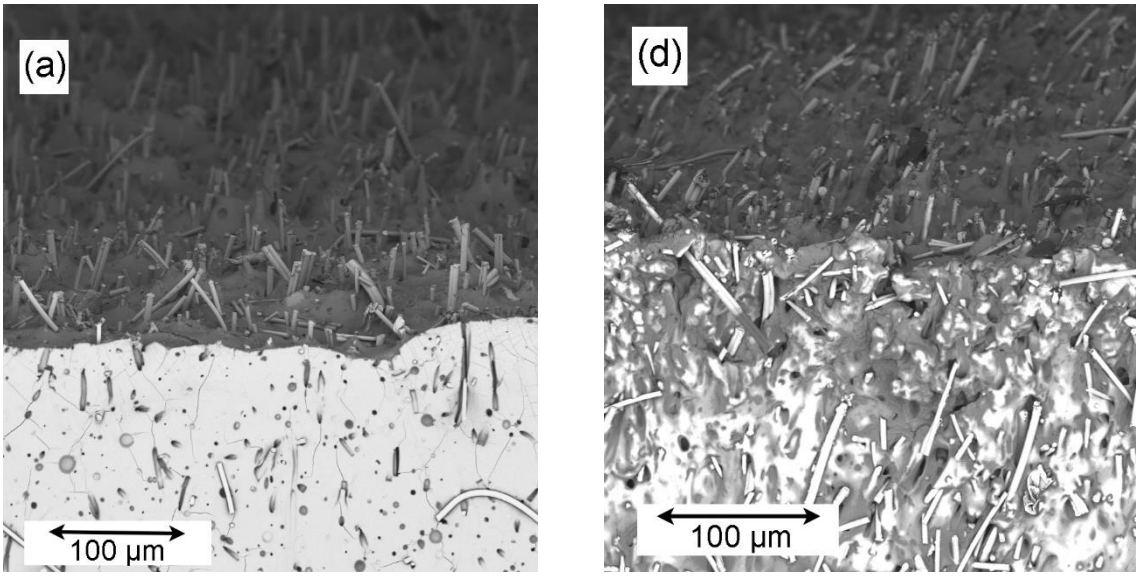

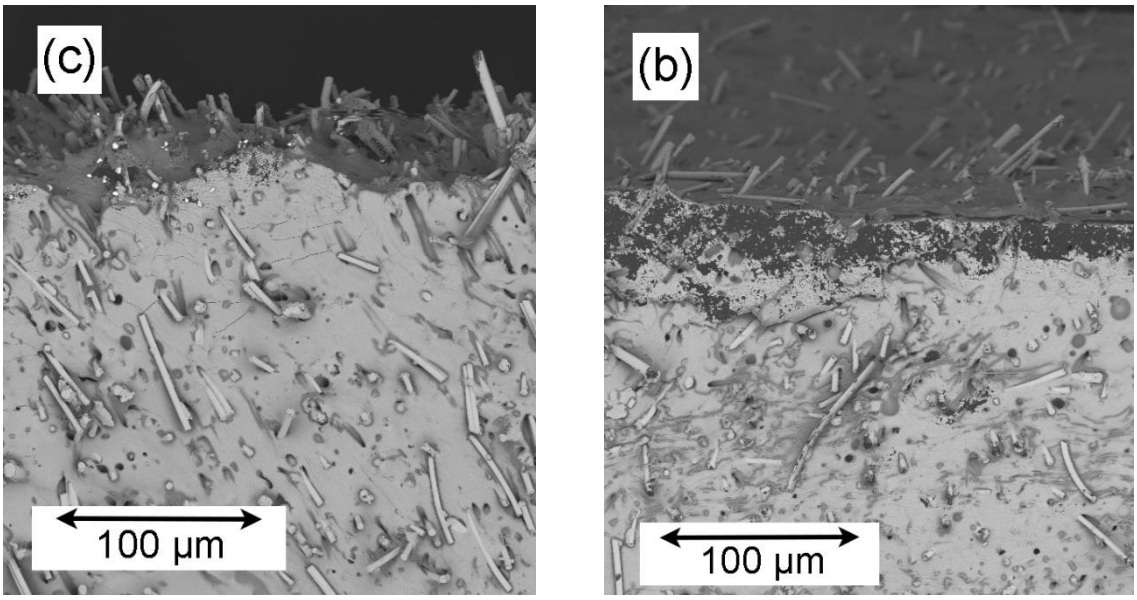

Figure 6.3: SEM images of composites with the following fibre contents: (a) 5% (3 mins. Milling time), (b) 5% (7 mins.), (c) 10% (3 mins) and (d) 10% (7 mins.).

In order to explore this a little further, and to obtain information about the actual volume fractions of reinforcement, density measurements were carried out on all 7 materials. This was done by hydrostatic weighing, using deionized water as the immersion fluid (with a density of 0.987 g cm^{-3} at 20°C). The outcomes are shown in Table 6.1. The density value quoted by the supplier of the rubber is 1.006 g cm^{-3}, but in fact the measured value was slightly higher than this, and so was taken as the correct fully dense value. The alumina (particulate and fibres) was taken to have a density of 3.99 g cm^{-3}. As reported in Chapter 5, the measured densities of the particulate composites were close to the corresponding fully dense values, suggesting porosity levels of just over 1%. As might have been expected, the fibre-reinforced composites contained slightly higher porosity levels, particularly with the higher of the two fibre contents and the lower of the two aspect ratios (longer milling time). This effect should be borne in mind, although the porosity levels are all relatively low and are unlikely to have a marked effect on the mechanical characteristics. Of course, it is also possible that the actual fibre levels differed somewhat from the nominal levels, although again it seems unlikely that the errors involved are very large.

Material	Densities (g cm^{-3})		Standard Errors	Inferred porosity Level (%)
	Measured	Expected		
Unfilled rubber	1.01	1.015	0.002	(0)
10 vol% Al_2O_3 particles	1.30	1.317	0.008	1.3
20 vol% Al_2O_3 particles	1.59	1.614	0.12	1.5
5 vol% Al_2O_3 fibres (7min.)	1.14	1.168	0.14	2.4
5 vol% Al_2O_3 fibres (3min.)	1.15	1.168	0.009	1.5
10 vol% Al_2O_3 fibres (7min.)	1.21	1.317	0.054	8.1
10 vol% Al_2O_3 fibres (3min.)	1.27	1.317	0.024	3.6
Al_2O_3	-	(3.99)		(0)

Table 6.1: Densitometry data for the 7 materials.

6.1.3 Mechanical Testing

Two types of tests were carried out, in each case on all 7 types of material and at 3 different temperatures (20°C, 45°C and 65°C). These were, firstly, conventional tensile stress-strain curve measurement (in the elastic regime) and, secondly, tensile creep testing under a fixed load.

6.1.3.1 Tensile Testing

The tensile testing was carried out using a Tinius Olsen H25KS universal tester and the details are presented in Chapter 4. All samples were about 90-100 mm long, with a gauge length of about 75 mm. During these tests, which were carried out relatively quickly (within about 30 s), the deformation was almost entirely elastic. As emphasized before, the large strains that arise during (elastic) deformation of rubbers create substantial differences between nominal and true stresses and strains. The classical rubber elasticity, Equation (2.3), only uses the nominal stress and strain but here the required true stress and strain were given by using Equation (2.6).

6.1.3.2 Creep Testing

Creep tests were carried out using the customized set-up described in Chapter 5. The system was first equilibrated thermally by switching on the heater, which was governed by one of the three thermocouples in contact with the sample. This was done with the sample under a small load – just the weight of the scale-pan. It was confirmed that the time needed for thermal equilibrium was short (~5-10 minutes). Once the sample was thermally stable, the load was quickly applied to the scale pan. A short period then followed during which the system reached the mechanical equilibrium, which probably involved a degree of settling and load redistribution in the gripping system and loading train, as well as some oscillation. The extension measured during this period of mechanical equilibration (typically a few tens of seconds) was not primarily arising from actual creep of the sample, so it was neglected when calculating the creep strain.

For the unfilled rubber and the two particulate composites, the loads used were 9.8 N, 11.8 N and 14.7 N, corresponding to nominal stresses of 0.17 MPa, 0.21 MPa and 0.26 MPa. For the fibrous composites, which exhibited considerably greater creep resistance, the loads were increased to 14.7 N, 17.6 N and 19.6 N (nominal stresses of 0.26 MPa, 0.31 MPa and 0.35 MPa). Of course, the corresponding true stress levels at the start of the creep test depended on the sample stiffness, which was measured from the tensile testing.

6.2 Experimental Results

6.2.1 Tensile Testing Results

Figure 6.4 shows the stress-strain plots obtained at room temperature, expressed as (a) nominal and (b) true values. The former was obtained by converting load and displacement data to stresses and strains, while the latter were obtained by applying Equations (2.5) and (2.6) to these data. For the unfilled rubber, and for the fibre composites, these tests were taken to final rupture, but this was not done for the

particulate composites, which were tested to about 30-40% strain. This is not so important, since it can be seen (Figure 6.4(b)) that they are all quite close to being linearly elastic, at least up to (true) strains of about 60-80%, which covers the range of interest here. A single Young's modulus value can thus be ascribed to each of them, as shown in Figure 6.4(b). As was noted previously for the unfilled rubber and for the particulate composites, the dependence of this value on temperature is small over the range concerned.

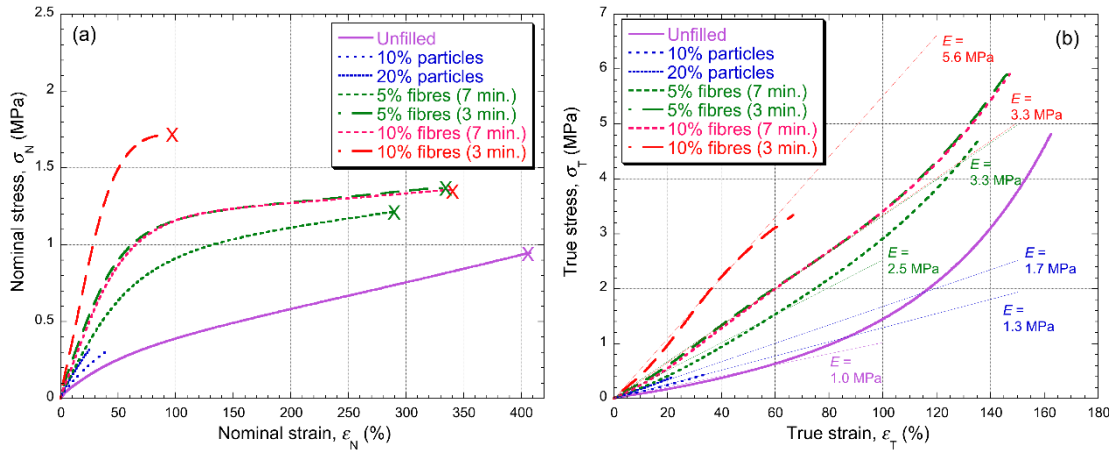

Figure 6.4: Stress-strain data from tensile tests on all 7 materials at 20°C, plotted as (a) nominal and (b) true values (with approximate values of the effective Young's modulus also shown).

It was also noted previously that the experimental (nominal) stress-strain curve for the unfilled rubber conformed well to the classical (entropy-dominated) rubber elasticity curve of Equation (2.3) that was used to obtain an estimate for n of $6.5 \times 10^{25} m^{-3}$.

The stiffening effects produced by both particulate and fibre additions are broadly consistent with predictions from the Eshelby model, more details of which are available in the literature [13, 61-63]. This can be seen in Figure 6.5(a), which shows a comparison between measured and modelled Young's moduli for all 6 of the composite materials. The elastic constants used in the model are shown in Table 6.2. It can be seen that the data for the particulate composites are consistent with the presence of equiaxed

particles (ie spheres, s = 1), as expected, while those for the fibrous composites are consistent with aspect ratios (s) of about 16 and 10 respectively for the short (3 mins.) and long (7 mins.) milling times respectively. This is also broadly in line with the microstructural observations (Figures 6.2 and 6.3), accepting that the fibre alignment is not perfect, which would tend to reduce the effective aspect ratio. These values of s have thus been taken to be representative (for both volume fractions) of the reinforcement architecture in these two types of composites.

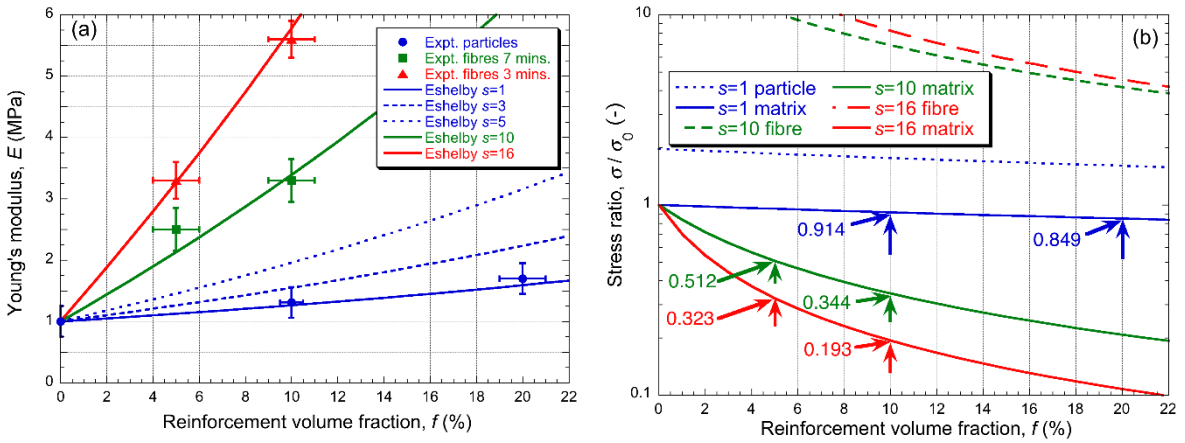

Figure 6.5: Eshelby model predictions for alumina spheres and prolate ellipsoids in a rubber matrix. As a function of reinforcement volume fraction, showing (a) Young's modulus (with measured values also shown) and (b) ratio of the stress in the two constituents to an applied tensile stress.

Material	Young's modulus, *E*(GPa)	Poisson ration, *v* (-)
Rubber	0.001	0.48
Al_2O_3	300	0.22

Table 6.2: Elastic constants used in the Eshelby modelling.

The plots in Figure 6.5(b) show predicted values for the (uniform) stress in the reinforcement and the (average) stress in the matrix, as a function of the reinforcement volume fraction, for these three aspect ratios (s = 1, 10 and 16). These stresses are shown as ratios to an applied true tensile stress, parallel to the axis of fibre alignment. These ratios are marked on the plot for the 6 cases of interest here. It can be seen that, as expected, stress transfer from matrix to reinforcement, at a given value of *f*, is much

more marked for the fibres than for the particulate. The matrix is thus being relieved of stress more effectively in the fibre-reinforced composites. Among other effects, this is expected to make those materials more resistant to creep than the particulate composites, for a given reinforcement content.

6.2.2 Creep Testing Results

The Miller-Norton law (Equation (3.5)), a model that captures both primary and secondary regimes of creep strain histories, with a smooth transition between them, is required in order to model the behaviour in this type of test (of relatively short duration).

The stress level used was taken to be the true value at the start of the creep (after the elastic deformation). This was obtained from the applied load by converting it to a nominal stress using the original sectional area and then applying Equation (2.4), knowing the nominal elastic strain (obtained from the plots in Figure 6.5(a)). The further (small) changes in true stress as the creep progressed were neglected.

6.2.2.1 Creep of Unreinforced Rubber

As reported in Chapter 5, it was found that the creep behaviour of the unfilled rubber conforms well to the Miller-Norton formulation (Equation (3.5)), using appropriate values for the parameters m and n, with the value of C being adjusted for the different test temperatures. The plots concerned, for the 3 different levels of applied stress, are shown in Figure 6.6. Furthermore, from the values of C found to give the best fit for the 3 temperatures, the activation energy, Q, was found to be ~7.4 kJ mol $^{-1}$. Of course, this is only a rough estimate, but the fact that it is a relatively low value is indicative of the rate-determining process being one of molecular reorganization, such as an untangling process, rather than involving rupture of cross-links or backbone bonds.

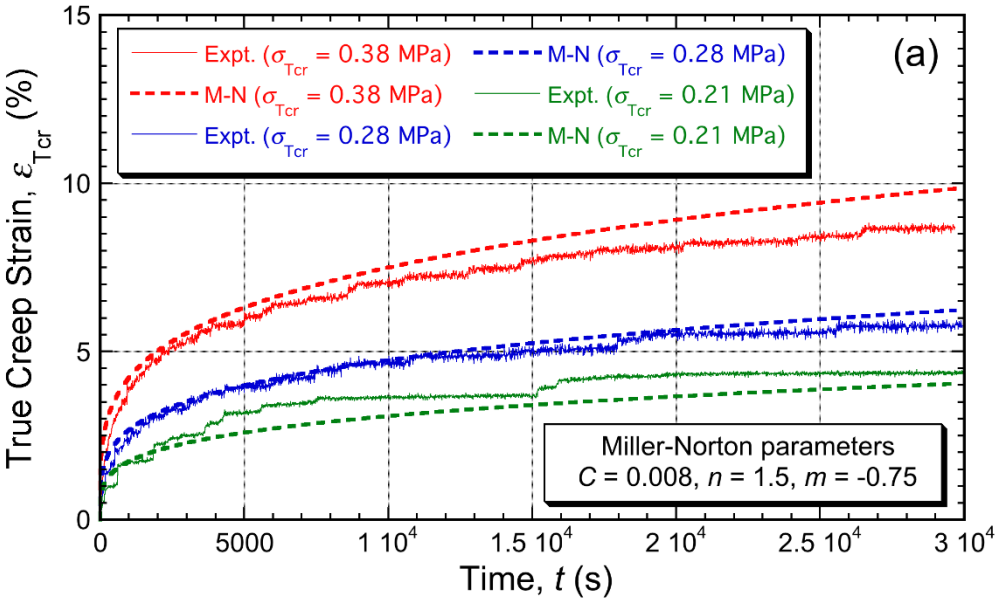
Expt. (σ_{Tcr} = 0.38 MPa)
M-N (σ_{Tcr} = 0.28 MPa)
M-N (σ_{Tcr} = 0.38 MPa)
Expt. (σ_{Tcr} = 0.21 MPa)
Expt. (σ_{Tcr} = 0.28 MPa)
M-N (σ_{Tcr} = 0.21 MPa)
(a)
Miller-Norton parameters
C = 0.008, n = 1.5, m = -0.75
True Creep Strain, ε_{Tcr} (%)
Time, t (s)
0
5
10
15
0
5000
1 10^4
1.5 10^4
2 10^4
2.5 10^4
3 10^4

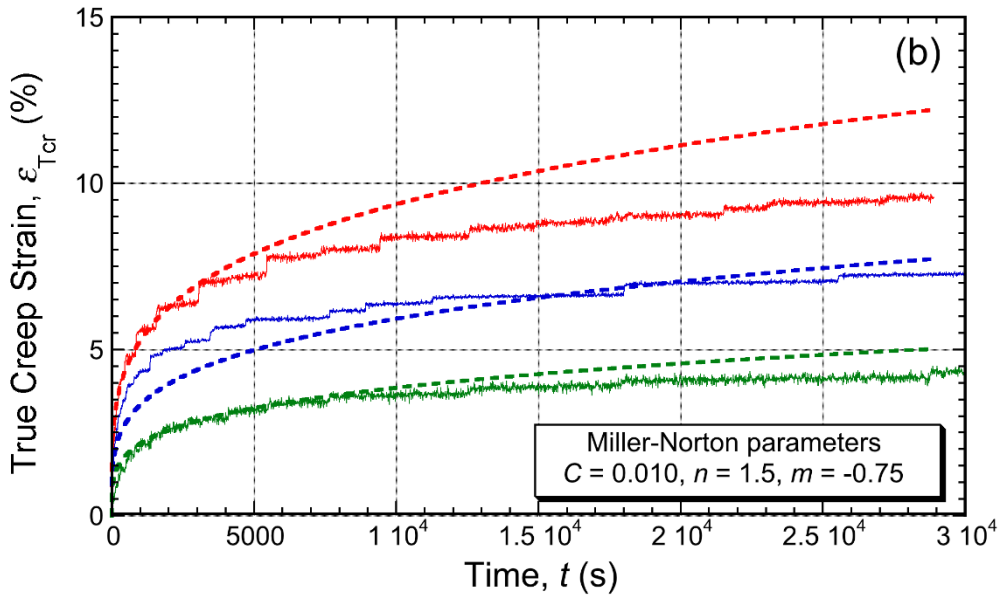
(b)
Miller-Norton parameters
C = 0.010, n = 1.5, m = -0.75
True Creep Strain, ε_{Tcr} (%)
Time, t (s)
0
5
10
15
0
5000
1 10^4
1.5 10^4
2 10^4
2.5 10^4
3 10^4

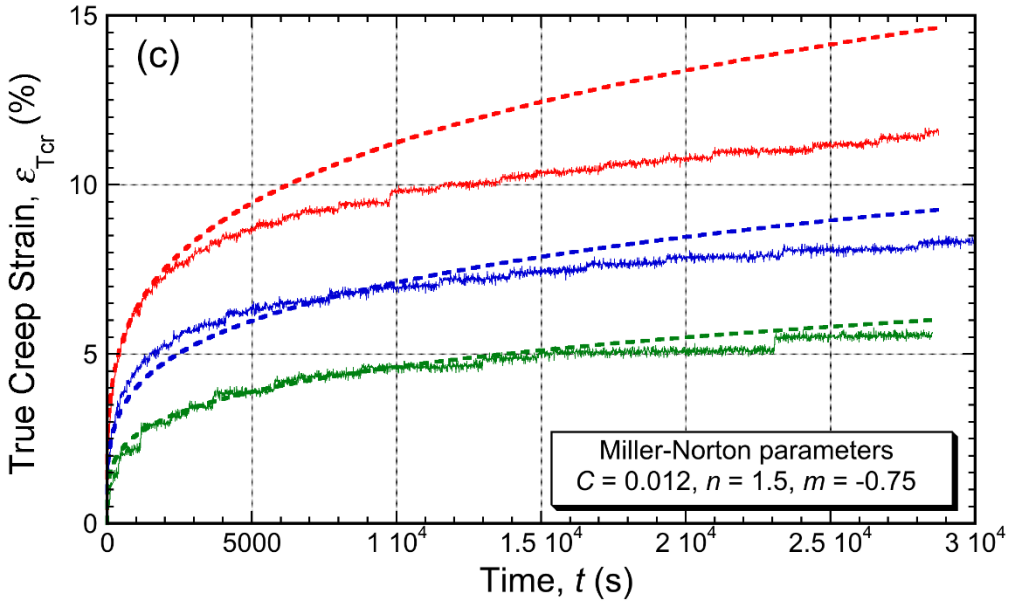

Figure 6.6: Measured and modelled creep strain histories for the unfilled rubber at (a) 20°C, (b) 45°C and (c) 65°C. The values of the initial true stress (after elastic deformation) are shown in the legend of Figure 6.6(a).

6.2.2.2 Creep of Composite

The greater stiffness levels of the composites, compared with the unreinforced rubber, meant that the elastic strains were lower and so the true stresses (acting at the start of the creep testing) were also lower. This effect is additional to that of the creep rate being reduced in the composites by the average stress in the matrix being lower than that acting on the sample as a whole (recognizing that creep only takes place in the matrix). This was studied in the Chapter 5 for the (s=1) particulate composites. Good agreement was observed between experiment and prediction for the creep strain histories by using the (Eshelby-predicted) average matrix stress in the Miller-Norton model, and taking account of the reduced volume of the sample in which the creep was occurring. In fact, while those composites did exhibit noticeably better creep resistance than the unfilled rubber, the differences were not dramatic, even at the 20% addition level. This is consistent with the associated enhancement in stiffness being fairly moderate (from 1 MPa to 1.7 MPa – see Figure 6.5(a)) and the reduction in average matrix stress also being relatively small (multiplied by a factor of about 85% - see Figure 6.5(b)).

The focus of Chapter 6 is on the behaviour of the fibre-reinforced composites. In these cases, even at the 10% addition level, the stiffness enhancement is substantial (from 1 MPa to about 5.6 MPa for the higher aspect ratio fibres - see Figure 6.5(a)) and the corresponding reduction in average matrix stress is also pronounced (to about 19% for that composite - see Figure 6.5(b)). The reductions in creep rate are thus expected to be appreciably greater with the fibrous reinforcement. This is quantitatively explored here, using the same type of analysis - i.e., the Miller-Norton formulation, using the same parameter values as those found appropriate for the unfilled rubber, with the matrix stress level being that obtained from the Eshelby model.

Figure 6.7 shows (for temperatures of 20°C and 65°C) experimental and predicted creep curves for the 5% composite containing fibres that had been milled for 7 minutes (such that the average fibre aspect ratio in the composites was about 10 – see Figure 6.5(a)). For the applied nominal stresses of 0.26 MPa, 0.31 MPa and 0.35 MPa, the nominal strains at the start of the creep tests were about 16.8%, 20.5% and 23.5% (true strains of 15.5%, 18.6% and 21.1%) and the corresponding true stresses were 0.30 MPa, 0.37 MPa and 0.42 MPa. Using the "stress reduction factor" of 0.512 for this composite (Figure 6.5(b)), these give average matrix stresses for use in the Miller-Norton equation of 0.154 MPa, 0.189 MPa and 0.215 MPa. While the agreement is naturally not perfect, it can be seen that the experimental creep data are broadly consistent with this modelling approach, capturing the effects of both applied stress and temperature. Corresponding plots for the other three fibre-reinforced composites are shown in Figures 6.8 – 6.10. These predicted curves were obtained using the multipliers shown in Figure 6.5(b) to obtain the average matrix stress levels. The plots were also multiplied by factors of 0.95 or 0.90, to take account of the effect of the creep taking place only in those volume fractions of the samples. It can be seen that the level of agreement is again good in all cases.

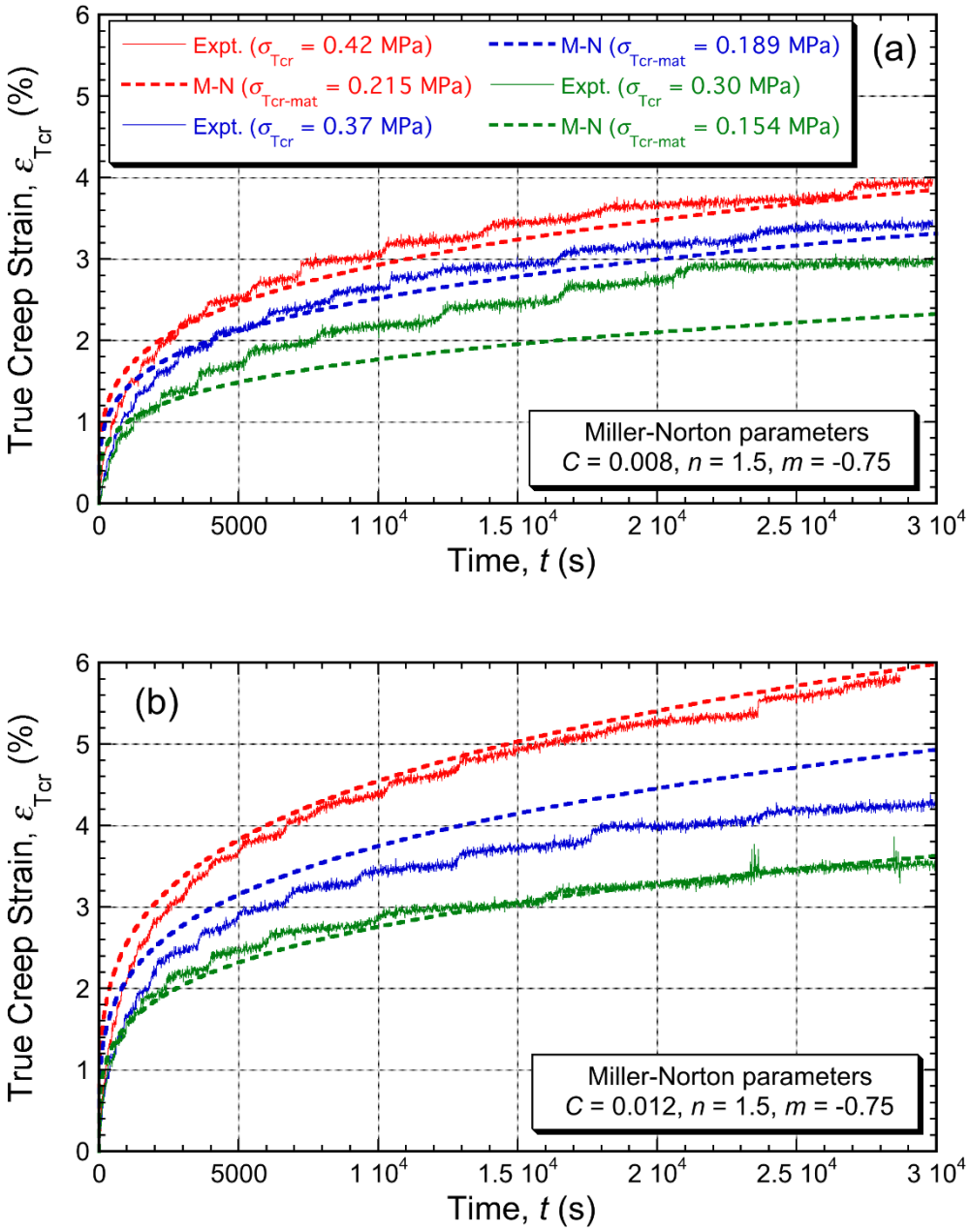

Figure 6.7: Measured and modelled creep strain histories for the 5% fibrous composite (7 mins. milling time) at (a) 20°C and (b) 65°C. initial true stress values are shown in the legend of Figure 6.7(a), as are the average values in the matrix (used in the M-N model).

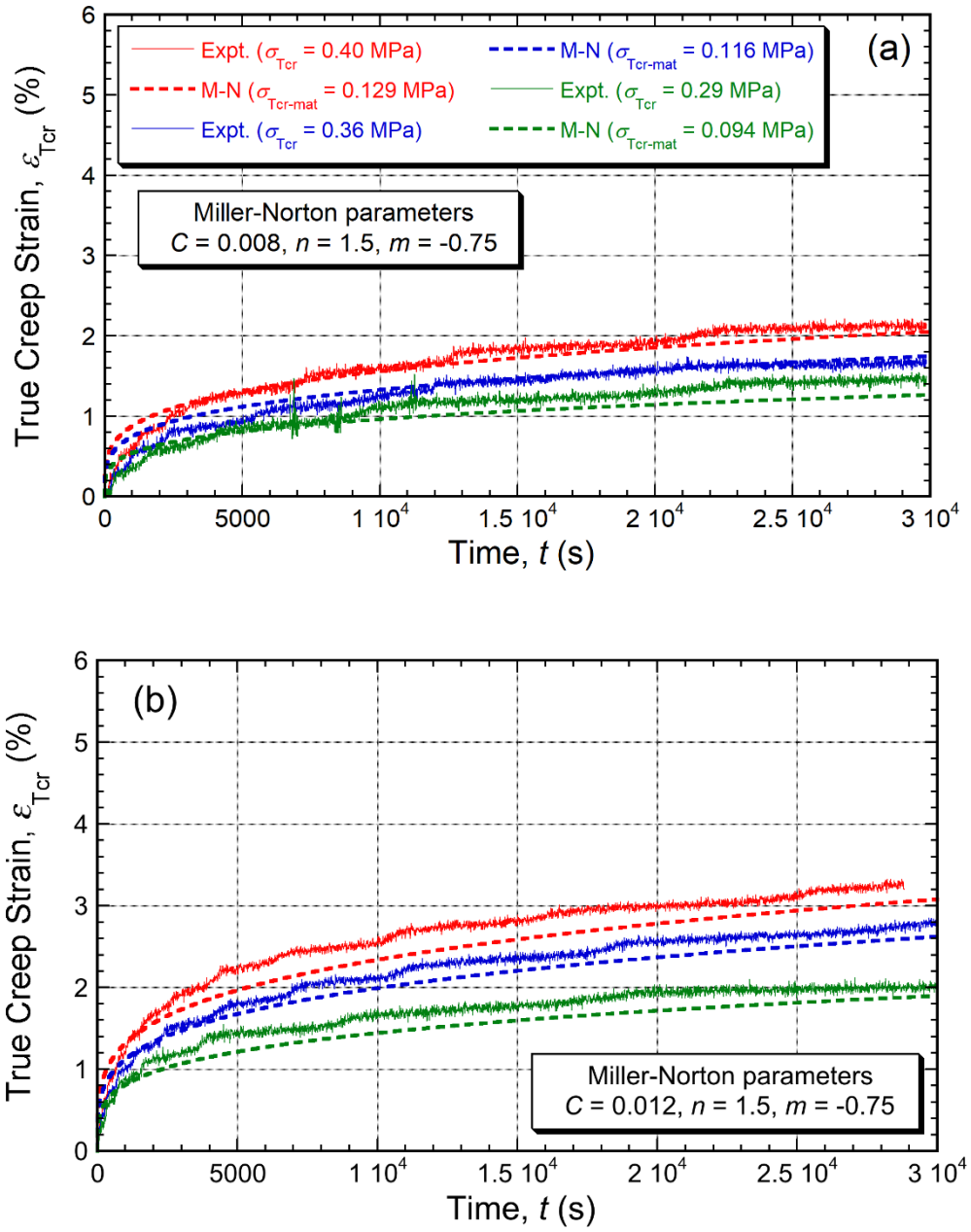

Figure 6.8: Measured and modelled creep strain histories for the 5% fibrous composite (3 mins. milling time) at (a) 20°C and (b) 65°C. Initial true stress values are shown in the legend of Figure 6.8(a), as are the average values in the matrix (used in the M-N model).

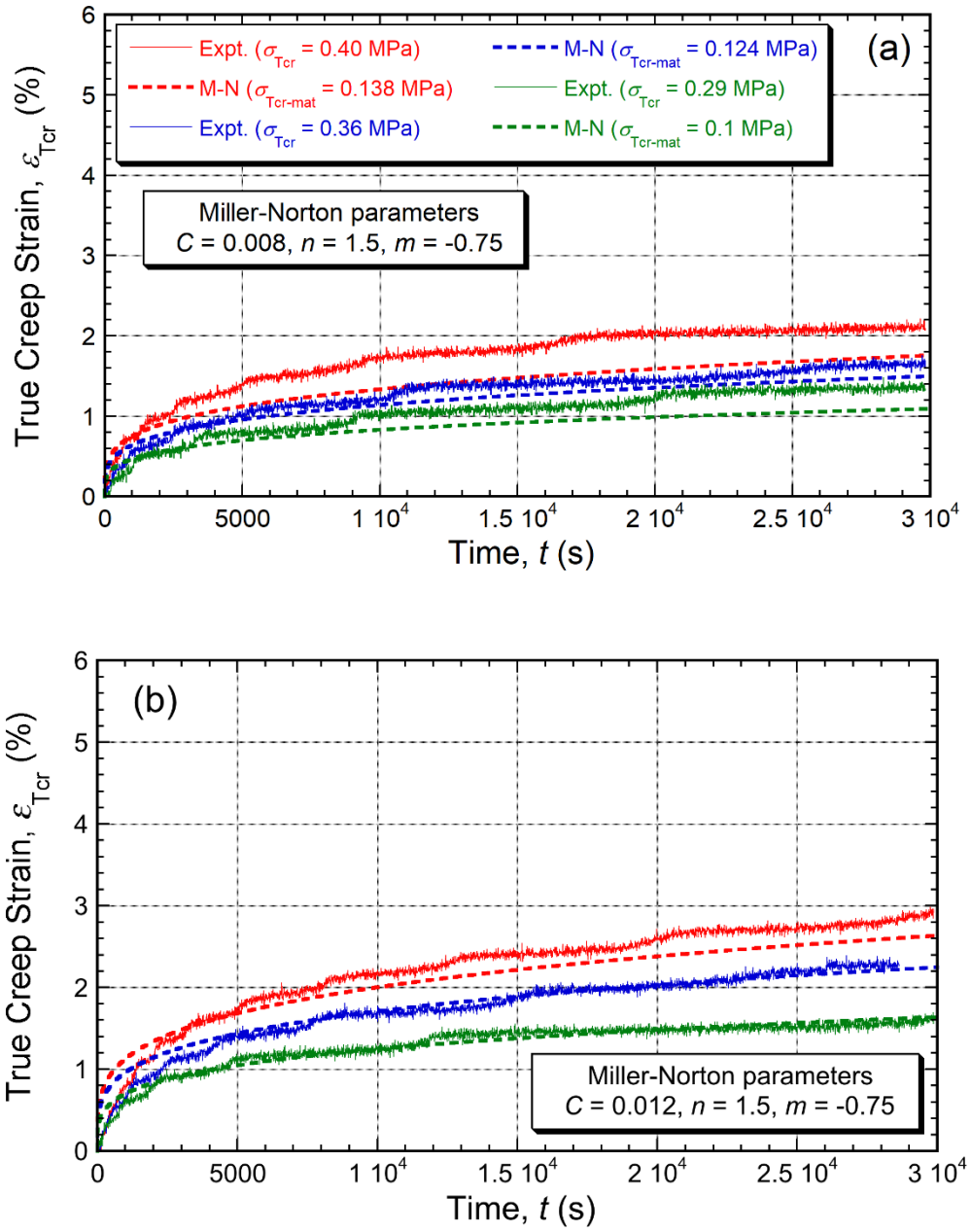

Figure 6.9: Measured and modelled creep strain histories for the 10% fibrous composite (7 mins. milling time) at (a) 20°C and (b) 65°C. Initial true stress values are shown in the legend of Figure 6.9(a), as are the average values in the matrix (used in the M-N model).

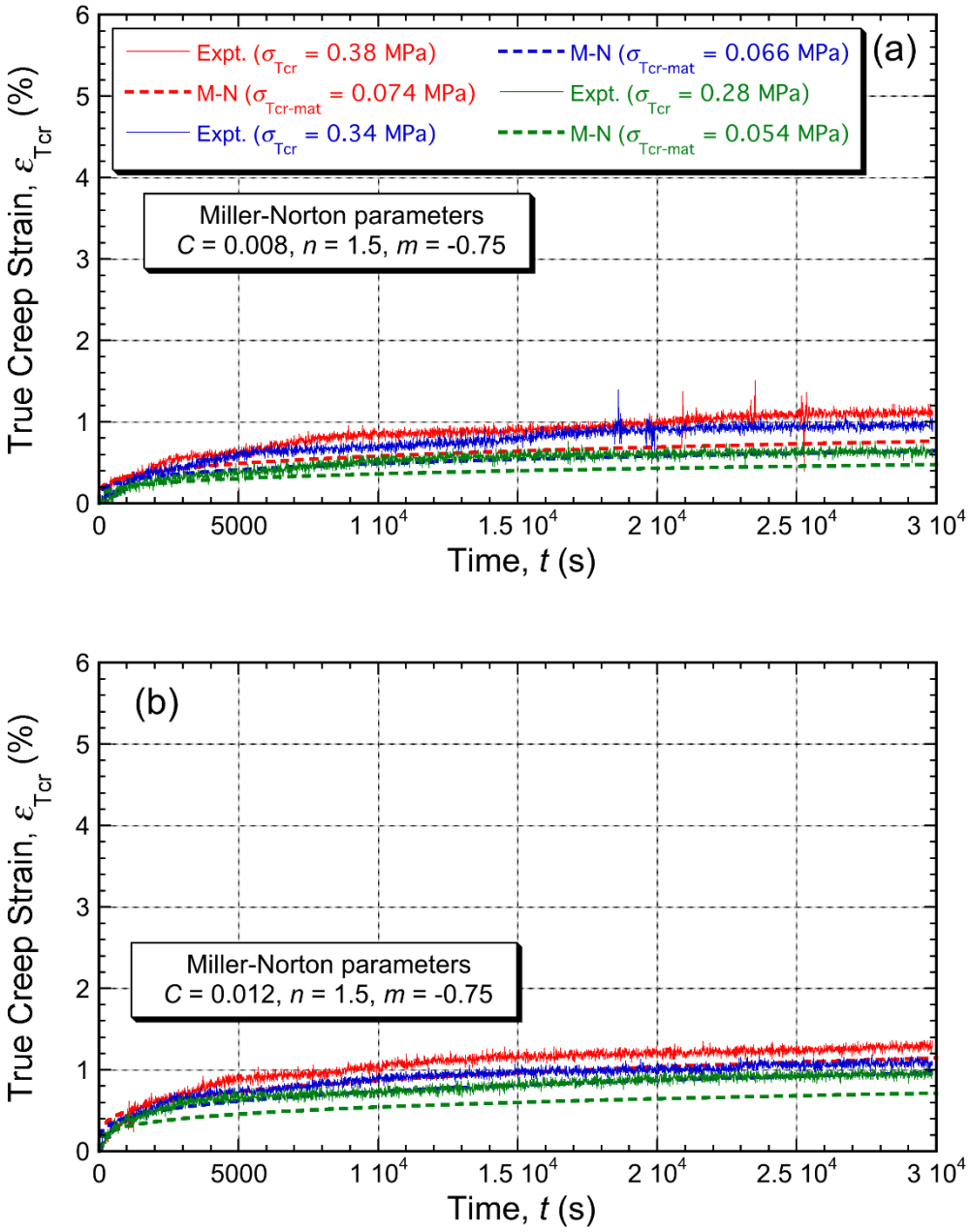

Figure 6.10: Measured and modelled creep strain histories for the 10% fibrous composite (3 mins. milling time) at (a) 20°C and (b) 65°C. Initial true stress values are shown in the legend of Figure 6.10(a), as are the average values in the matrix (used in the M-N model).

It is certainly striking that creep is much more strongly inhibited in the fibrous composites, compared with the particle-reinforced materials. For example, with an applied nominal stress of 0.26 MPa at 20°C (a condition used for all materials), the total creep strain after a period of 3×10^4 s (about 8 hours) is about 8.5% for the unfilled

rubber, 6% for the 10% particulate composite and 4% for the 20% particulate composite. For the fibrous composites, on the other hand, the figures are about 3%, 2%, 1.4% and 0.6% (respectively for two 5% contents and the two 10% contents). Put another way, at the 10% addition level, the presence of the particulate effects a relatively small reduction (of about 30%) in the creep strain of the rubber, whereas fibres can cut it down by over 90%.

Chapter 7
Creep of Composites based on Silicone Rubber

Chapter 5 and Chapter 6 concerned the creep of PU rubber, with and without reinforcement, as a function of applied stress and temperature. There is also an interest in the creep behaviour of pure silicone rubber, and also silicone rubber with short fibre filling since they have been used in some wide-ranging industrial applications, for example, seals, gaskets, damping systems, in which they endured prolonged loads, gamma radiation and relatively high temperature [64-66].

The creep behaviour of unfilled and short fibre filled silicone rubbers might be different, in contrast with the polyurethane rubber. They can be produced with the same manufacturing procedures and the effect of the fibrous fillers may follow the same trend of the prediction by the Eshelby model. In addition experimental creep histories of these materials may be captured by using the Miller-Norton law. A further investigation of unfilled and filled silicone rubber is described in this Chapter in an effort to confirm whether these possibilities might be correct.

7.1 Experimental Procedures

7.1.1 Silicone rubber - Dow Corning SE 1700

Silicone rubbers are polymers that combine siloxane (Si-O-Si unit backbones) with another organic group, such as methyl, vinyl or phenyl groups [67]. They are normally colourless rubber-like substances. The terminology for the silicone rubbers is polydimethylsiloxane (PDMS). The main chain of silicone rubber is siloxane bonding (Si-O). It carries 106.0 kcal/mol bond energy, while carbon bond, C-C, only carries 84.9 kcal/mol, which gives the siloxane bond greater strength and stability. Consequently, silicone rubber shows better heat resistance, electric insulation and chemical stability than other organic rubbers [68]. The stability of the siloxane bond comes from the sharp difference between Si and O in terms of electronegativity making Si-O closer to an ionic bond. Since silicone chain molecules are helical and their intermolecular force low, silicone rubber has high elasticity, high compressibility and excellent resistance to cold temperatures [69]. In addition, it is odourless, tasteless, and chemically stable.

In this work, the type of silicone rubber used is Dow Corning SE 1700 (reinforced polydimethylsiloxane), supplied by DOW chemical company limited in Japan. It is made from two components, which are Part A, PDMS (white paste), and Part B (transparent catalyst liquid), the mix ratio for Part A and B is 10:1. The chemical formula for Part A (PDMS), is $CH_3[Si(CH_3)_2O]_nSi(CH_3)_3]$ where n is the number of repeating monomer $[SiO(CH_3)_2]$ units [70]. For Part B, Dodecamethylcyclohexasiloxane (D6), which is used as curing agent, the chemical formular is $C_{12}H_{36}O_6Si_6$. The features of this product are non-flowing (high viscosity, 542 Pa-Sec), heat cure (curing at 150°C), high tensile strength (6.8 MPa), and good working time (8 hours at 25°C) after mixing. The benefits of this product are rapid, versatile cure processing controlled by temperature, and long working time reduces need for equipment clean-up.

7.1.2 Sample Preparation

The three types of material tested were unfilled silicone rubber, and silicone rubber with 5 and 10 vol % fibrous addictions. The fibrous composites were made from mixing ''Saffil'' (alumina fibres) and Dow Corning SE 1700 (silicone rubber matrix).

The alumina fibres were received as chopped fibre mats, supplied by Saffil Ltd (Widnes), and the diameter of the fibres was about 3 μm. The fibres were relatively long, in the mm range in as-received form. For blending, mixing, and testing purposes, they needed to be chopped into μm in length. Therefore, a short milling procedure, in the ball mill (DECO All-Direction Planetary Ball Mill), was employed to reduce fibres length. The whole milling process has been described in Chapter 6. The milling times were set to 3 minutes only. The fibre length was measured by using optical microscopy and freeware (ImageJ). The short fibres with the higher aspect ratio were collected for producing the fibrous composite rubbers.

The mixing process of unfilled SE 1700 was simply to put Parts A and B with the 10:1 mix ratio, by weight, into a sample bag. After sealing, the bag was kneaded and squeezed for about 45 minutes [71, 72]. In order to avoid the air entrapment, the mixture was kept in a sealed container and evacuated under a soft 25 to 30 inches Hg vacuum for 10 minutes after the squeezing to reduce trapped air.

For making the homogeneous fibrous composite rubbers, SE 1700 Parts A and B with the ratio 10:1 by weight, were weighed separately. After that, Part A and short fibres were mixed with a ratio of 10:4.9, by weight, for 10 vol % composite, or mixed in a ratio of 10:2.3, by weight, for 5 vol % composite. Each was sealed into a sample bag, kneaded, and squeezed for 45 minutes. After this process, Part B liquid was injected into each mixture bag by syringe. Subsequently, the mixtures containing Parts A and B, and short fibres, were mixed and further kneaded and squeezed for another 45 minutes. As with the unfilled silicone rubber, these mixtures needed to be kept in a sealed container and be run through an air evacuation process for 10 minutes.

Both extraction and moulding of the unfilled and filled rubber mixes were carried out in the same way. A hypodermic syringe with a 2 mm in diameter bore was employed to extract the viscous mixture paste. As shown in Figure 7.1, the inner diameter of the mould was about 8.5 mm, however, the length of the mould was reduced to about 85 mm since the higher viscosity of the mixture paste caused difficulty in extrusion. Both unfilled and filled rubber samples were demounted after 48 hours. After demounting, they needed to be cured in an oven and set temperature at 150 °C for 30 minutes and then at 145°C for 24 hours.

Figure 7.1: Photo of straw and syringe for producing samples.

7.1.3 Microstructural Characterisation

As in Chapter 6 fibres were found to align fairly well with the axis of the sample, although this alignment was naturally not perfect.

The extrusion paste based on silicone rubber was more viscous than the composite polyurethane rubber. Although the alignment of fibres wasn't perfect too, the orientation of fibres still tended to lie in the axial direction. This spatial distribution can be observed from Figure 7.2, which shows SEM micrographs of two types of composite silicone rubbers. These photos also show both a "cut" (lateral) and a "fracture"

(transverse) surface. Comparing with composite polyurethane rubber in Chapter 6, the alignment of fibres in silicone rubber was not less, but some porosity also could be seen in the silicone matrix from the photos.

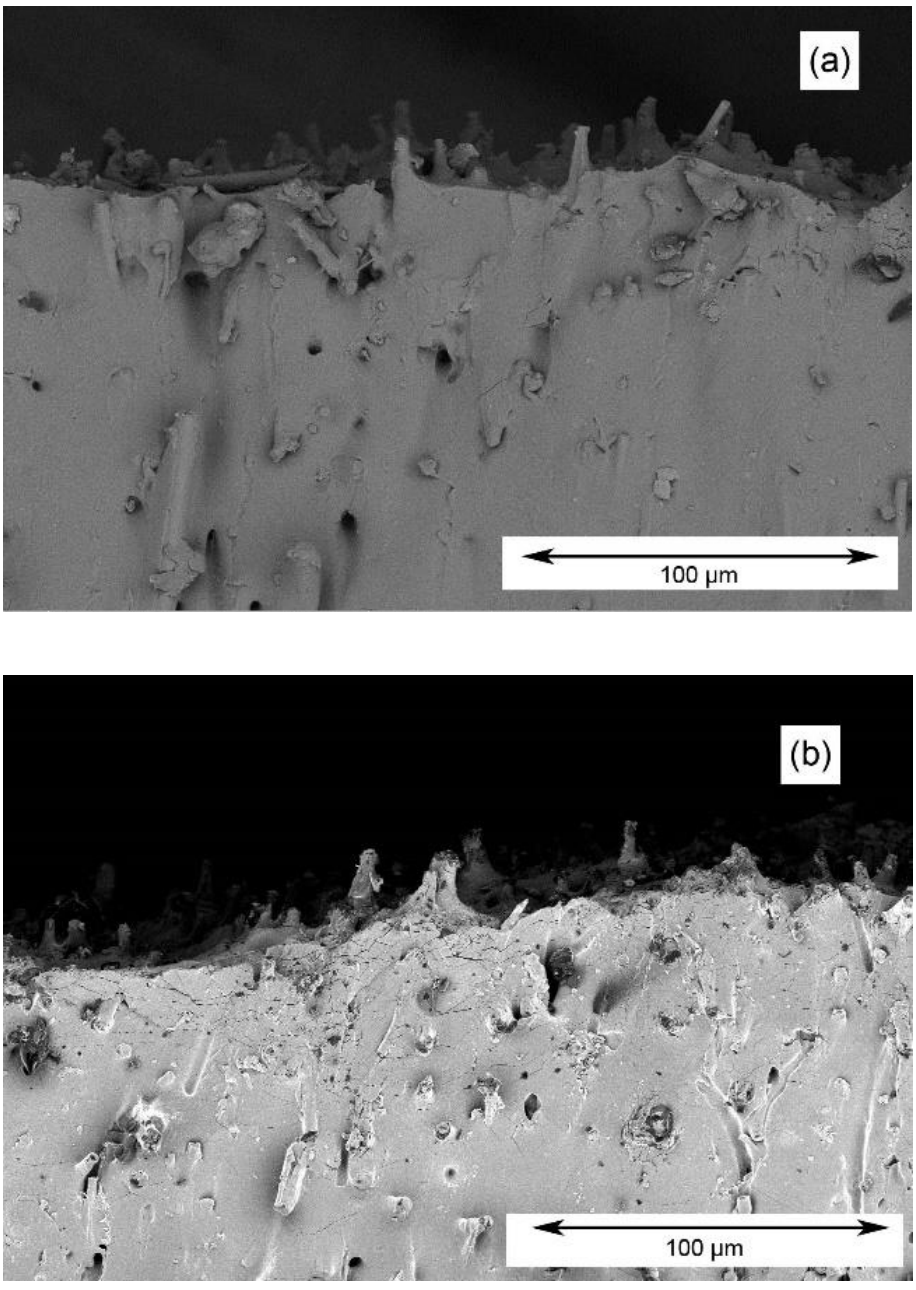

Figure 7.2: SEM images of composite with fibre contents: (a) 5% (3 mins. milling time), and (b) 10% (3 mins. milling time).

The density value of SE 1700 quoted from the supplier is 1.13 g cm $^{-3}$. The alumina fibres were taken to have a density of 3.99 g cm $^{-3}$. The measured densities of these three

materials, which were done by hydrostatic weighing, using deionized water as the immersion fluid (with a density of 0.987 g cm^{-3} at 20°C), are shown in Table 7.1. As in Chapter 6, the fibre-reinforced composites contained slightly higher porosity levels, particularly with the higher of the two fibre contents. The manufacturing process worked appropriately since the porosity levels were acceptably low and thus unlikely to have a marked effect on mechanical characteristics.

Material	Densities (g cm^{-3})		Standard Errors	Inferred porosity Level (%)
	Measured	Expected		
Unfilled rubber	1.11	1.13	0.01	1.8
5 Vol% Al_2O_3 fibres (Milling time 3 mins.)	1.22	1.27	0.25	3.9
10 Vol% Al_2O_3 fibres (Milling time 3 mins.)	1.36	1.42	0.3	4.2

Table 7.1: Densitometry data for the 3 materials.

7.2 Mechanical Testing

Tensile and creep tests were carried out on these three materials, namely unfilled silicone rubber, 5 and 10 vol% filled composite silicone rubbers. Firstly, the tensile testing was carried out at 20 °C, following by tensile creep testing under a fixed load at 20 °C and 65 °C.

7.2.1 Tensile Testing

The tensile testing was run by using a Tinius Olsen H25KS universal tester with a constant displacement rate of 1.67 mm s^{-1} until the fracture took place in the sample. It

took about 30 s, which was corresponding to an approximate strain rate of 0.02 s^{-1}, similar to the range in Chapter 5. The sample was about 8.5 mm in diameter, the total length was about 60 – 70 mm, and the gauge length was about 40 mm. The deformation was almost entirely elastic.

As previously mentioned, the large strains that arise during elastic deformation of rubbers could create substantial differences between nominal and true stress and strain. Thus nominal stress and strain were converted to true stress and strain by using Equations (2.4) and (2.5).

7.2.2 Creep Testing

The tensile creep tests of silicone rubber and silicone rubber composites were carried out using the customised set-up rig described in Chapter 4.

Pre-test thermal and mechanical equilibrium are also important for silicone rubber even though it is stiffer than polyurethane rubber. Therefore, the sample was hung with the scale pan and pre-heated up to the test temperature (65 °C) for 5 to 10 minutes, monitored by three thermocouples touching the sample, before quickly adding the loads to the scale pan.

For the filled and unfilled silicone rubber, the applied loads were 14.7 N, 17.6 N and 19.6 N. Hence, the nominal stresses of unfilled rubbers were 0.26 MPa, 0.31 MPa and 0.35 MPa, and the corresponding true stresses were 0.29 MPa, 0.36 MPa and 0.41 MPa, all of which were acquired right after the initial elastic deformation. The true stresses within filled rubbers varied depending on volume percentage of the fibres in the matrix. For 5 vol% composite rubber, they were 0.263 MPa, 0.317 MPa and 0.354 MPa. For 10 vol% composite rubber, they were 0.261 MPa, 0.314 MPa and 0.350 MPa. It was evident that fracture and slippage did not occur in either unfilled or filled samples during the test. The loading quickly generated elastic extension, consequently a short period followed during which the system reached mechanical equilibrium. Therefore,

the extension measurement for the period of mechanical equilibration (a few tens of seconds) was discounted when plotting the graph of creep strain versus time.

7.3 Experimental Results

7.3.1 Tensile Testing Results

Figure 7.3(a) and (b) shows the stress-strain plots at room temperature, expressed as nominal values (solid lines) and true values (dashed lines). The nominal values could be obtained by converting load and displacement data to stresses and strains, while the true values were acquired by applying Equation (2.5) and (2.6) to these data. It also can be seen in Figure 7.3 (b) that the true stress-strain plot of the unfilled rubber is close to linear elastic and both plots of the composite rubbers are linear elastic. In addition, the true stress-strain plots almost overlap the nominal stress-strain plots for the composite silicone rubbers when the stress level is less than 2 MPa. Thus, the stiffness of these materials is greater than the stiffness of composite polyurethane rubbers with and without the same fibre content.

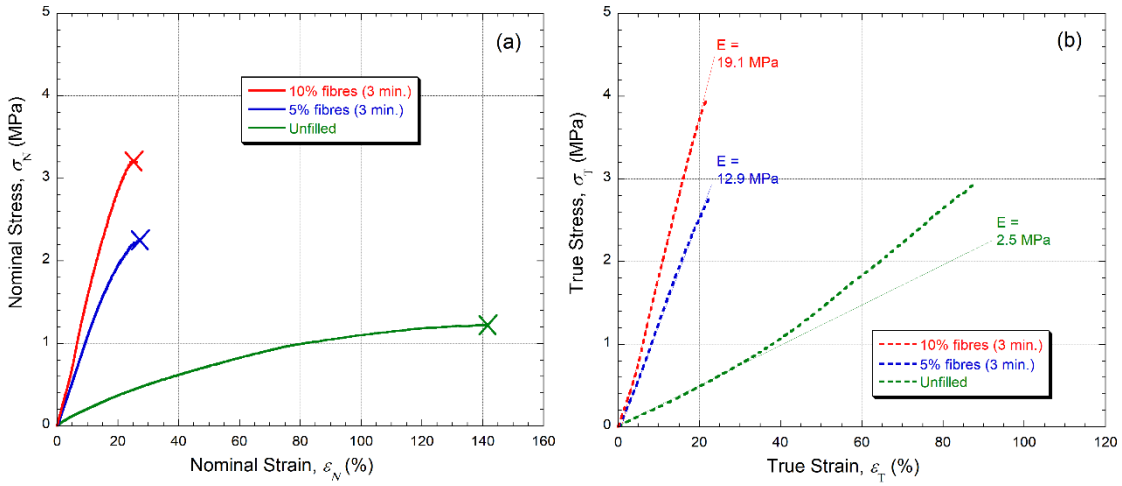

Figure 7.3: Stress-strain data from tensile test on all 3 materials at 20 °C, plotted as (a) nominal and (b) true values (with approximate Young's modulus).

It was also noted in Chapter 5 that experimental (nominal) stress-strain curves for the unfilled PU rubber conformed well to the classical (entropy-dominated) rubber

elasticity curve of Equation (2.3) and that was used to obtain an estimate for n of 6.5×10^{25} m $^{-3}$. In this case, the estimated n of 1.75×10^{26} m $^{-3}$ was acquired by using stress-strain plots for unfilled rubber (SE 1700) with Equation (2.3), see Figure 7.4. Consequently, it confirms that silicone rubber is stiffer than PU rubber. According to the plot, the Young's modulus of SE 1700 was established to be 2.5 MPa.

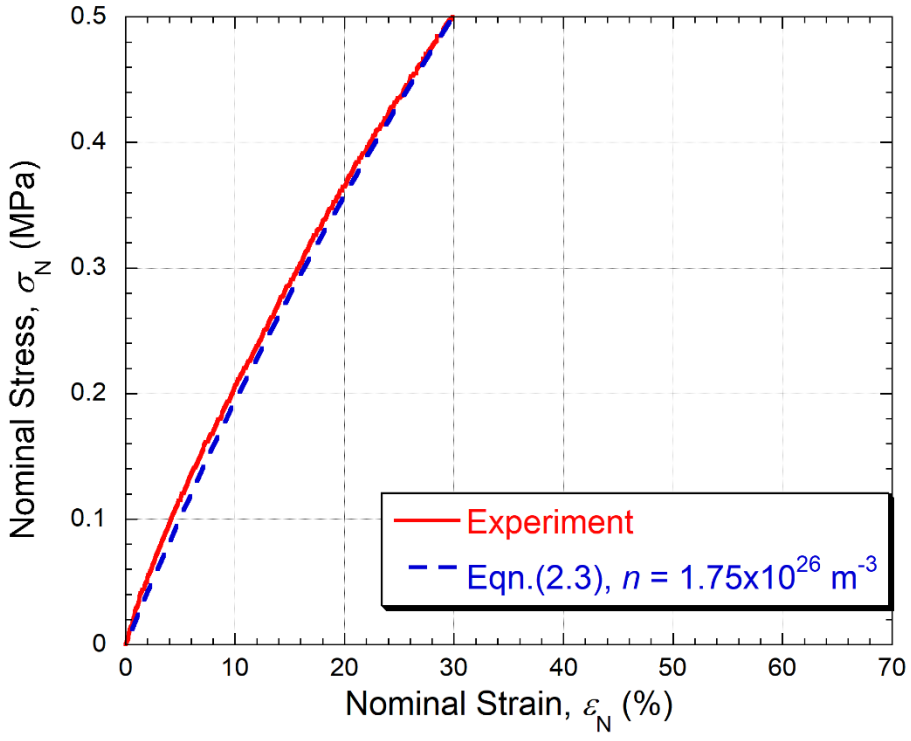

Figure 7.4: Comparison between the experimental nominal stress – nominal strain curve for the unfilled rubber at room temperature and predictions from the classical equation from rubber elasticity theory with the number of chain segments per unit volume (related to the cross-link density).

The stiffening effects produced by fibre additions can be seen in Figure 7.5 (a), which shows a comparison between the measured Young's moduli and the Eshelby model, based on the composite rubbers (silicone). The elastic constants used in the model are shown in Table 7.2. Those experimental data (solid square) for the fibrous composites are consistent with aspect ratios of about 20 for the short (3 mins.) milling time (solid line). This value of aspect ratio might also increase matrix stiffness, even if the alignment of the fibres were similar to that seen in Chapter 6.

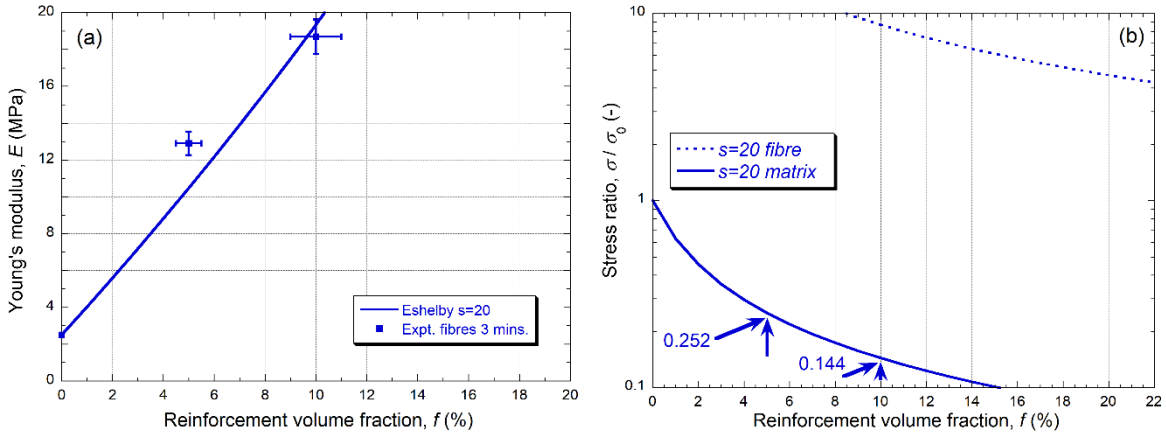

Figure 7.5: Eshelby model predictions for alumina prolate ellipsoids in rubber matrices, SE 1700, as a function of reinforcement volume fraction, showing (a) Young's modulus (with measured values also shown) and (b) ratio of the stress in the two constituents to an applied tensile stress.

Material	Young's modulus, E (GPa)	Poisson ration, *v* (-)
Rubber (Silicone)	0.0025	0.48
Al_2O_3	300	0.22

Table 7.2 Elastic constants used in Eshelby modelling.

The plots in Figure 7.5 (b) show predicted values for the (uniform) stress in the reinforcement (fibres) and the (average) stress in the matrix. For a constant fibre aspect ratio (s = 20) in both silicone composite rubbers, the 'stress reduction factors' were 0.252 with 5 vol% fibrous content and 0.144 for the 10 vol% fibrous composite rubber.

7.3.2 Creep Testing Results

As shown in Chapter 5 and Chapter 6, for capturing both primary and secondary regimes of creep strain curves with a smooth transition, the Miller–Norton model is employed, Equation (3.5).

The stress applied to the specimen at the start of creep was the true value and was taken right after initial elastic deformation. It was calculated from the applied load by

using Equation (2.4). Since the samples were stiffer, the further changes of true stresses as creep progressed were insignificant, thus they were neglected.

7.3.2.1 Creep of Unreinforced Silicone Rubber

The creep characteristics can be represented quite well by using the Miller-Norton formulation, which uses appropriate values of the parameters *m*, *n* and adjusted value *C* for different test temperatures (20 °C and 65 °C), shown in Figure 7.6(a) and (b).

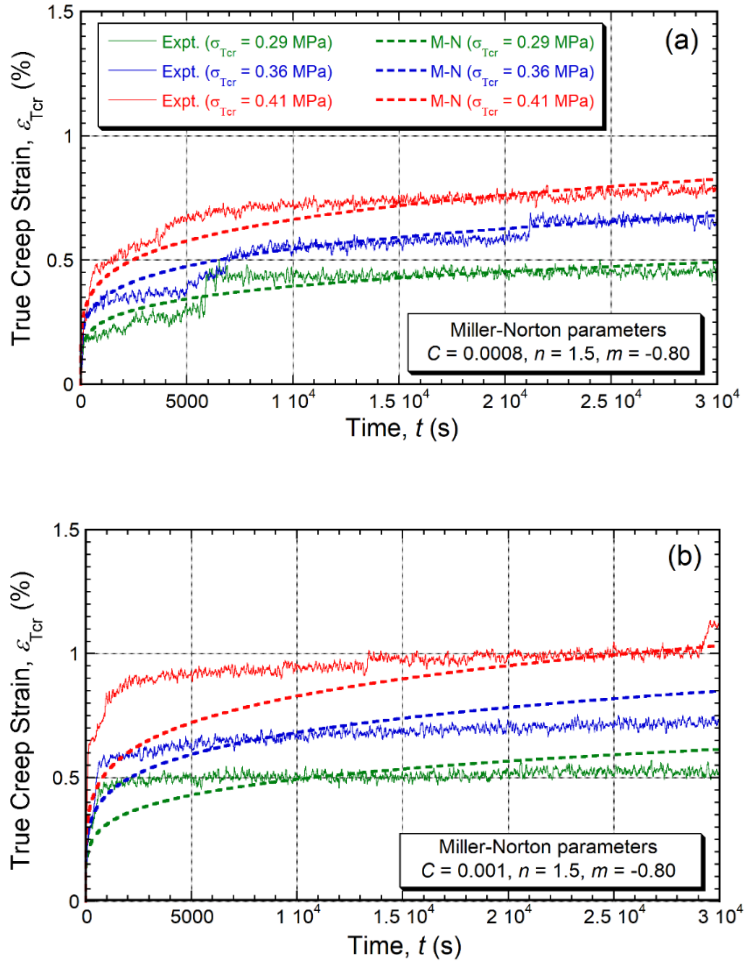

Figure 7.6: Measured and modelled creep strain histories for the unfilled silicone rubber at (a) 20°C and (b) 65°C. The values of the initial true stresses are shown in the legend of Figure 7.6(a).

7.3.2.2 Creep of Composite Silicone Rubber

Comparing with the unfilled PU rubber, the stiffness level of unfilled silicone rubber was greater, and its elastic strain lower. Hence, the fibrous composite silicone rubber was also stiffer than both particulate composite and fibre composite PU rubbers. Furthermore, the true stresses in silicone rubber were lower than in the PU fibre composite rubbers for the same attached loads (which were 14.7 N, 17.6 N and 19.6 N). The true stresses in unfilled silicone rubber were 0.29 MPa, 0.36 MPa and 0.41 MPa right after the elastic deformation while nominal stresses were 0.26 MPa, 0.31 MPa and 0.35 MPa. Similarly, for the 5 vol% fibrous composite silicone rubber, the true stresses were 0.26 MPa, 0.32 MPa and 0.35 MPa and for the 10 vol% fibrous composite silicone rubber, they were 0.26 MPa, 0.32 MPa and 0.35 MPa. The previous work in Chapter 6 showed good agreement between experiment and prediction of the true creep strain histories while applying (Eshelby-predicted) average true stress in the matrix for using the Miller-Norton model. The same approach was therefore taken with silicone rubber.

The foregoing results in Figure 7.5(a) indicated that composite silicone rubber was significantly stiffer than equivalent composite PU rubber. Furthermore, the corresponding 'stress reduction factor' for s = 20 fibrous composite silicone rubbers, shown in Figure 7.5(b), were 0.252 for 5 vol% and 0.144 for 10 vol% fibre contents. Therefore, the true creep stresses became 0.067 MPa, 0.081 MPa and 0.088 MPa in the matrix of 5 vol% composite silicone rubber and 0.037 MPa, 0.046 MPa and 0.052 MPa in the matrix of 10 vol% composite silicone rubber. Figures 7.7 and 7.8 show that average true matrix stresses in the Miller-Norton model only fairly agreed with the true creep experimental strain curves, however. But it is worth noting that fine experimental creep strain histories are not easily measured using a long stroke LVDT in conditions where the average stresses in the matrix are so low. In addition, these plots were also multiplied by factors of 0.95 or 0.90 respectively, which are the matrix factors for the 5 vol% and 10 vol% samples.

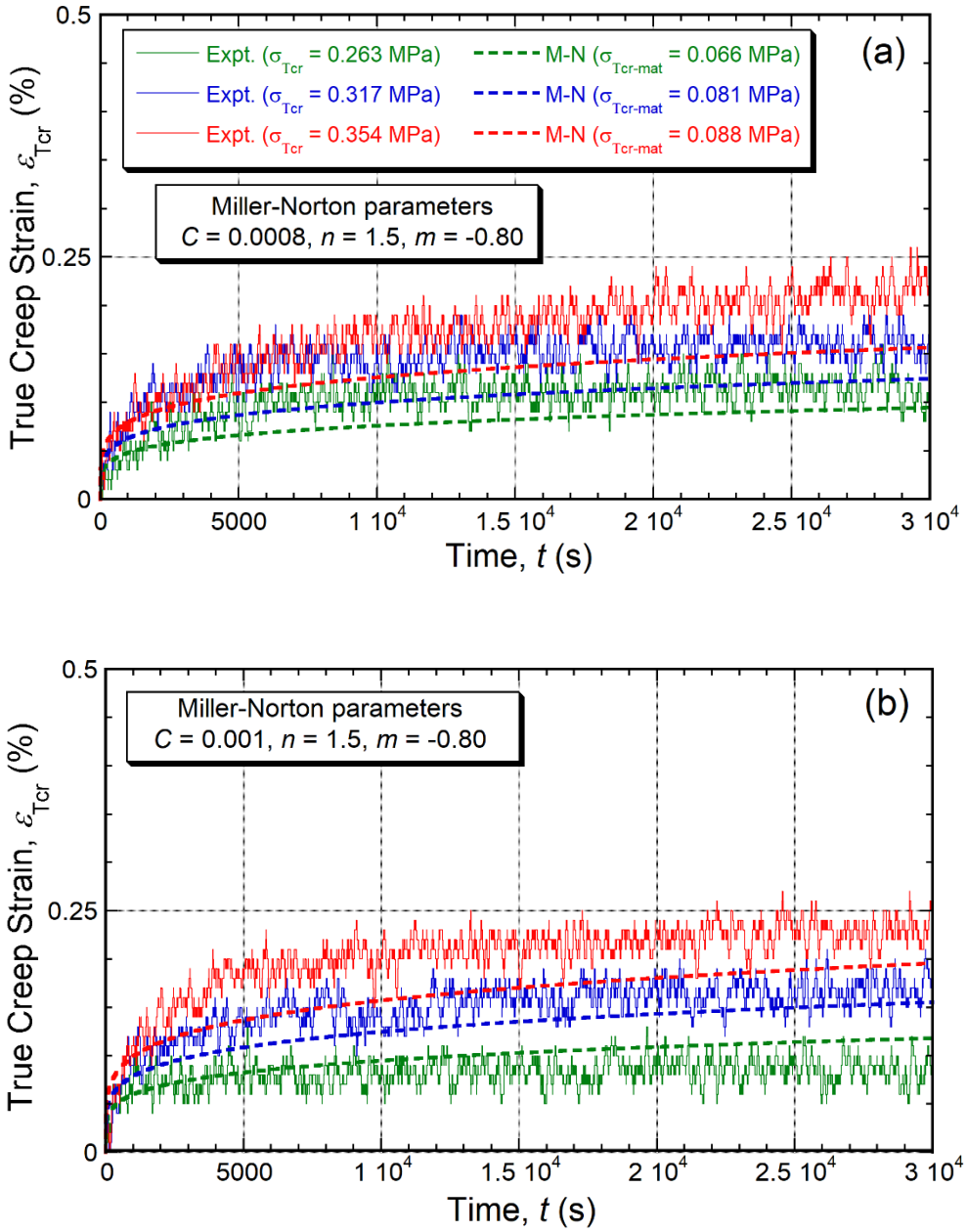

Figure 7.7: Measured and modelled creep strain histories for the 5% fibrous composite (3 mins, milling time) at (a) 20 °C and (b) 65 °C. Initial true stress values are shown in the legend of Figure 7.7(a), as are the average values in the matrix (used in the M-N model).

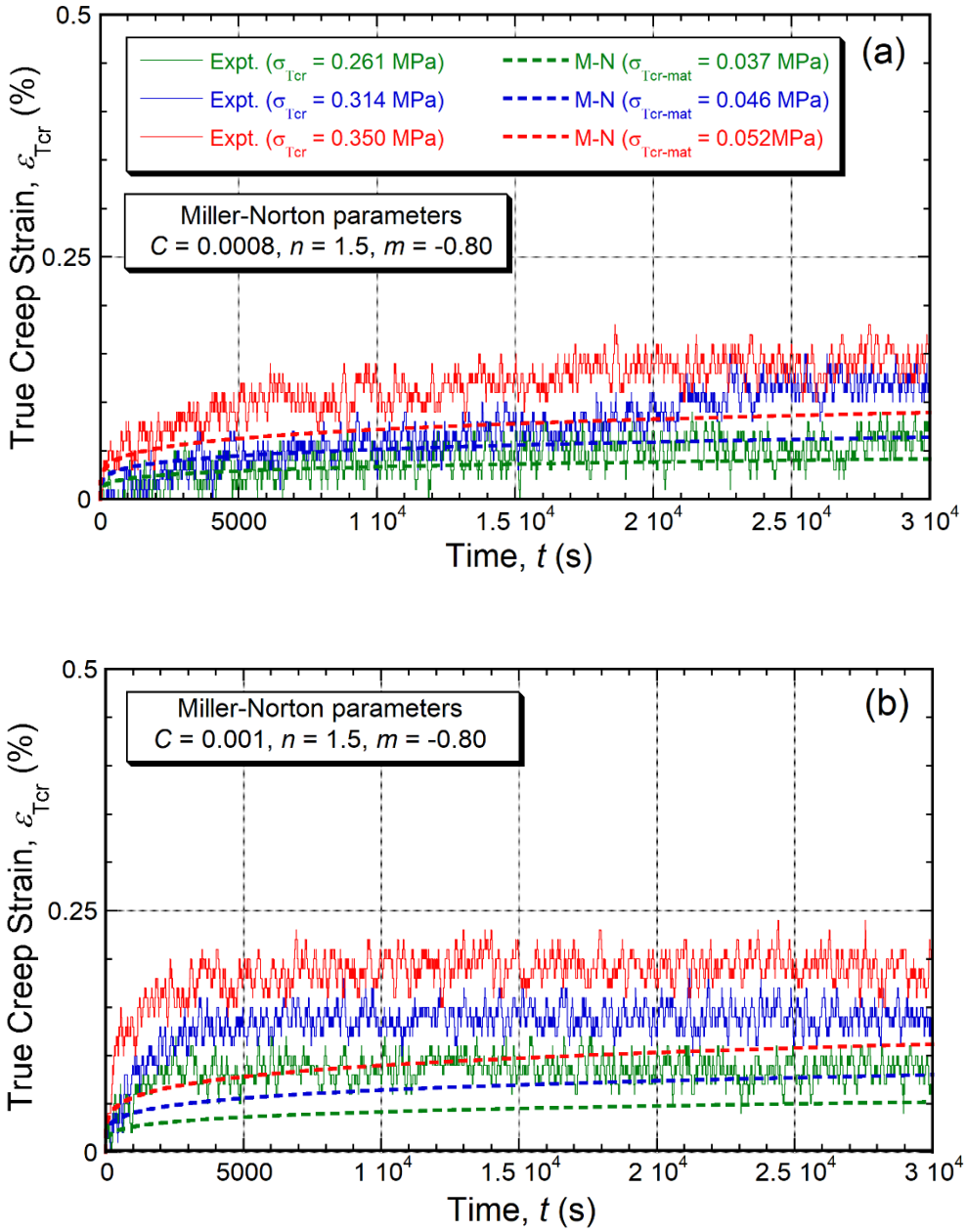

Figure 7.8: Measured and modelled creep strain histories for the 10% fibrous composite (3 mins, milling time) at (a) 20 °C and (b) 65 °C. Initial true stress values are shown in the legend of Figure 7.8(a), as are the average values in the matrix (used in the M-N model).

It is crystal clear that the creep resistance and stiffness of silicone rubber is significantly better than the PU rubber. Hence, the creep resistance of the fibrous composite silicone rubber is also better than both the particulate composite PU rubber and the fibrous composite PU rubber. As Chapter 5 and Chapter 6 show, for example,

with an applied nominal stress of 0.26 MPa at 20°C, the total true creep strain after 3104 s (about 8 hours) is about 8.5% for the unfilled PU rubber, 6% for the 10 vol% particulate composite PU rubber and 4% for the 20 vol% particulate composite PU rubber. For the fibrous composite PU rubbers, they are a maximum of 2% and 0.6% for 5 vol% and 10 vol% content, respectively. For the unfilled and filled silicone rubbers, these figures are 0.44% for the unfilled silicone rubber, 0.2% for the 5 vol% fibrous composite silicone rubber and 0.15% for the 10 vol% fibrous composite silicone rubber. Remarkably creep strain could be cut down by 90% and 75% in 5 vol% and 10 vol% fibres content if polyurethane rubber matrix were replaced by silicone rubber in the matrix.

Chapter 8

Conclusions

Overall, this is the first time that the Miller-Norton constitutive law is employed to study the creep behaviour of rubber and rubber composite, which are non-metal materials. The creep historical strains of all these rubbers and rubber composites have been well captured by using this empirical formulation, which is normally only used for predicting the creep behaviour of metal materials. Therefore, this work may give a convenient way to capture the creep behaviour of rubber and rubber composite compared to the conventional method, e.g. Prony series. Furthermore, there are more details in findings about creep behaviours of rubbers and rubber composites which are presented below.

8.1 Creep of Particulate PU Rubber

(a) Samples of polyurethane rubber, with and without 10 vol% or 20 vol% of alumina particulate filler, have been subjected to both tensile (stress-strain) testing (in the elastic regime) and tensile creep (constant load) testing, at three different temperatures (up to 65°C).

(b) A small amount of (primary) creep may have slightly affected the tensile stress-strain curves, but in general they were consistent with the classical theory of rubber elasticity, allowing the number of chain segments per unit volume to be estimated as ~6 x $10^{25}m^{-3}$. Furthermore, plotted as true stress–strain values, all three materials exhibited approximately linear elastic behaviour, at least up to

strains of several tens of %. The enhancement of Young's modulus resulting from the presence of the filler was consistent with composite elasticity theory.

(c) It was found that the (primary and secondary) creep characteristics of the rubber could be well captured using the Miller-Norton formulation. The dependence on temperature of the parameter expected to be sensitive to it was found to be consistent with Arrhenius behaviour, with an activation energy of about 7 kJ mol $^{-1}$. This (relatively low) value is thought to indicate that the rate-determining process during creep is predominantly a physical process, without breaking either cross-links or backbone bonds.

(d) It is noted that, for a given applied (nominal) stress, the higher stiffness of the filled rubbers results in a lower elastic strain and hence a lower true stress at the start of the creep test. (The reverse would have been true if the testing had been carried out in compression.) This is expected to result in a lower creep rate. However, the results confirm that, in addition to this effect, the composites have a greater inherent creep resistance than the unfilled rubber.

(e) It has been shown that the improved creep resistance of the composites is consistent with the predicted load transfer to the particles, reducing the average matrix stress. Since this load transfer is relatively small (for the addition levels used), the creep resistance of the composites is not vastly greater than that of the unfilled rubber, although there is certainly a significant effect.

8.2 Creep of Fibre - Reinforced PU Rubber

(a) Samples of polyurethane rubber, with and without alumina reinforcement (as short fibres, mainly aligned in the loading direction, at levels of 5 and 10 vol%), have been subjected to both tensile (stress-strain) testing (in the elastic regime) and tensile creep (constant load) testing, at three different temperatures (up to 65°C).

(b) Plotted as true stress–strain values, all seven of the materials exhibited approximately linear elastic behaviour over the strain range of interest (up to about 80%). The effective values of the Young's moduli for the composites were

found to be consistent with predictions from the Eshelby (equivalent homogeneous inclusion) model, with the particles taken to be spheres and the fibres to be prolate ellipsoids with the same aspect ratios.

(c) The creep strain curves, measured over a period of about 8 hours, were found to fit well in all cases with predictions obtained using the Miller-Norton equation, including the dependence on temperature and applied stress (taken to be the true stress acting at the start of the creep period). The presence of the reinforcement thus reduces the creep rate of the unreinforced matrix via both the increase in stiffness (reducing the true stress acting on the sample) and the reduction in average matrix stress due to stress transfer.

(d) The stress transfer effect has been simulated using the Eshelby model, with the resultant average matrix stress used in the Miller-Norton equation (and account also taken of the reduction in the volume fraction of the sample in which the creep is occurring). The creep curves predicted in this way were in good agreement with experiment for all six of the composite materials, capturing the effect of the reinforcement aspect ratio, as well as volume fraction.

(e) A striking outcome of both the experiments and the simulations is that (short) fibres provide a much greater increase in creep resistance than particles (at a given reinforcement level). This is the case for both fibre aspect ratios used, but even the lower value ($s \sim 10$) has a strong effect. The production of composite material containing high (>~10%) fibre contents may be problematic, but the improvement in creep resistance is marked even for the levels studied here (5% and 10%). Furthermore, while this work has covered only composites with a degree of fibre alignment (along the loading direction), it is likely that isotropic material containing (low levels of) short fibres of this type will show strong improvements in creep resistance under multi-axial loading.

8.3 Creep of Composite based on Silicone Rubber

(a) Tensile creep (constant load) testing has been carried out for the samples of silicone rubber, with and without alumina short fibres (both milling time 3 mins,

aspect ratio, s ~ 20, aligned in the loading direction, at content levels of 5 vol% and 10 vol%) at 20 °C and 65 °C. The tensile (stress-stain) testing (in elastic regime) for these materials was only run at room temperature (20 °C).

(b) Plotted in true stress-strain values, these three materials also showed approximately linear elastic behaviour over the strain range of interest, which was up to about 30%. The measured Young's moduli for both of 5 vol% and 10 vol% composite silicone rubber were close to the predictions by using the Eshelby (equivalent homogeneous inclusion) model while the fibres were in prolate ellipsoids with the same aspect ratios (s ~ 20).

(c) The measured creep strain curves in the period of about 8 hours fairly matched those predictions that use Miller-Norton equation with applied stress at the started point of the creep period at the dependent temperatures. The embedded fibres as reinforcement significantly cut the creep rate of the unreinforced matrix through both increasing the stiffness (reducing the true stress in the sample) and decreasing the average stress in matrix as a result of the stress transfer.

(d) The stress transfer has been simulated by using the Eshelby model, and the resultant average stress in the matrix was employed in the Miller-Norton equation. Since the matrix material was silicone rubber, the stress in the matrix was lower. The creep predictions for both composite silicone rubber materials fitted fairly with the experimental creep strain curves when taking account of the effect of the fibre aspect ratio, and volume fraction of the matrix.

(e) This work has shown that in comparison with polyurethane rubber silicone rubber has greater stiffness and higher creep resistances. Hence, as a new stiffer matrix material, the addiction of optimised micro-fibres could increase creep resistance significantly more.

8.4 Future Work

Although the results presented here are encouraging and promising, there is scope for future investigation into the creep behaviour of other rubbers, composite rubber materials, and other polymer-based materials. It would be useful if predictions from the

Miller-Norton model could be shown to match experimental creep strain histories data from a wide range of polymer and polymer-based materials.

In order to investigate the creep strain histories of different polymer-based materials, there is room to optimise the test set-up. For example, for finding out the activation energies of different rubber and composite rubber materials, the experimental temperature capability could be raised to around 100 °C once health and safety issues have been improved. Better stress-strain properties might be achieved from dumbbell shape specimens. Furthermore, better creep strain histories data might be obtained from a more accurate extensometer of varying sensitivity to cater for specimens of higher stiffness and small creep strains.

List of Publications

[1] Cui, Y, M Burley, JE Campbell, M Patel, K Hunt & TW Clyne, Effects of Temperature and Filler Content on the Creep Behaviour of a Polyurethane Rubber. Mechanics of Materials.,2020.148..

[2] Cui, Y & TW Clyne, Creep of Particle and Short Fibre Reinforce Polyurethane Rubber. MTDM., Accepted, (2021)

References

1. Plazek, D.J., *Effect of crosslink density on Creep Behavior of natural rubber vulcanates.* Journal of Polymer Science Part a-2-Polymer Physics, 1966. **4**(5PA2): p. 745-&.
2. Derham, C.J., *Creep and stress relaxation of rubbers - effects of stress history and temperature changes.* Journal of Materials Science, 1973. **8**(7): p. 1023-1029.
3. Ngo, A.T. and J.R. Valdes, *Creep of sand-rubber mixtures.* Journal of Materials in Civil Engineering, 2007. **19**(12): p. 1101-1105.
4. Oman, S. and M. Nagode, *Observation of the relation between uniaxial creep and stress relaxation of filled rubber.* Materials & Design, 2014. **60**: p. 451-457.
5. Sagar, G., D. Zheng, A. Suwannachit, M. Brinkmeier, K. Fietz, and C. Hahn, *On the Development of Creep Laws for Rubber in the Parallel Rheological Framework.* Tire Science and Technology, 2019. **47**(1): p. 2-30.
6. Derham, C.J. and A.G. Thomas, *Creep of rubber under repeated stressing.* Rubber Chemistry and Technology, 1977. **50**(2): p. 397-402.
7. Lee, B.S. and E.I. Rivin, *Finite element analysis of load-deflection and creep characteristics of compressed rubber components for vibration control devices.* Journal of Mechanical Design, 1996. **118**(3): p. 328-336.
8. Luo, R.K., *Creep modelling and unloading evaluation of the rubber suspensions of rail vehicles.* Proceedings of the Institution of Mechanical Engineers Part F-Journal of Rail and Rapid Transit, 2016. **230**(4): p. 1077-1087.
9. Chen, C.H. and C.H. Cheng, *Micromechanical modeling of creep behavior in particle-reinforced silicone-rubber composites.* Journal of Applied Mechanics-Transactions of the Asme, 1997. **64**(4): p. 781-786.

10. Daver, F., M. Kajtaz, M. Brandt, and R.A. Shanks, *Creep and Recovery Behaviour of Polyolefin-Rubber Nanocomposites Developed for Additive Manufacturing.* Polymers, 2016. **8**(12).
11. Banerjee, S.S. and A.K. Bhowmick, *High Temperature Thermoplastic Elastomers from Rubber Plastic Blends: A State-of-the-Art Review.* Rubber Chemistry and Technology, 2017. **90**(1): p. 1-36.
12. Ramachandran, P., J. Dutta, T. Chatterjee, G.B. Nando, and K. Naskar, *Investigation of different Cross-linking methods of EOC:PDMS Thermoplastic Elastomers for Cable Insulation Application with special reference to Thermal, Rheological, Creep and Electrical Properties.* Rubber Chemistry and Technology, 2017. **90**(4): p. 585-610.
13. Clyne, T.W. and D. Hull, *An Introduction to Composite Materials*. 3rd ed. 2019, Cambridge: Cambridge University Press.
14. Callister, W.D., *Materials Science and Engineering-An Introduction*. 4th ed. 1997: John Wiley and Sons. 852.
15. Ward, I.M., *Mechanical properties of solid polymers*. Second ed. 1983, Chichester: John Wiley & Sons.
16. Tsang, H.T., C.G. Chao, and C.Y. Ma, *Effects of volume fraction of reinforcement on tensile and creep properties of in-situ TiB/Ti MMC.* Scripta Materialia, 1997. **37**(9): p. 1359-1365.
17. Nardone, V.C. and J.K. Tien, *On the Creep Rate Dependence of Particle Strengthened Alloys.* Scripta Met., 1986. **20**: p. 797-802.
18. Whitehouse, A.F., H.M.A. Winand, and T.W. Clyne, *The Effect of Processing Route and Reinforcement Geometry on Isothermal Creep Behaviour of Particulate and Short Fibre MMCs.* Mat. Sci. & Eng., 1998. **A242**: p. 57-69.
19. Requena, G., D. Telfser, C. Horist, and H.P. Degischer, *Creep behaviour of AA 6061 alloy and AA 6061 metal matrix composite.* Materials Science and Technology, 2002. **18**(5): p. 515-521.
20. Gariboldi, E. and M. Vedani, *Creep damage behaviour of Al6061-Al2O3 particulate composites.* International Journal of Materials & Product Technology, 2002. **17**(3-4): p. 243-260.
21. Patel, M. and A.R. Skinner, *Thermal ageing studies on room-temperature vulcanised polysiloxane rubbers.* Polymer Degradation and Stability, 2001. **73**(3): p. 399-402.
22. Luo, R.K., *Creep prediction with temperature effect and experimental verification of rubber suspension components used in rail vehicles.* Proceedings of the Institution of Mechanical Engineers Part C-Journal of Mechanical Engineering Science, 2019. **233**(11): p. 3950-3963.

23. Eshelby, J.D., *The Determination of the Elastic Field of an Ellipsoidal Inclusion and Related Problems.* Proceedings of the Royal Society of London, 1957. **241**: p. 376-396.
24. Eshelby, J.D., *Elastic Inclusions & Inhomogeneities*, in *Prog. Solid Mech.*, I.N. Sneddon and R. Hill, Editors. 1961. p. 89-140.
25. Markenscoff, X. and A. Gupta, eds. *Collected Works of J. D. Eshelby (The Mechanics of Defects and Inhomogeneities)*. 1 ed. Solid Mechanics and Its Applications. 2006, Springer Netherlands. 939.
26. Huang, J.H., Y.H. Chiu, and H.K. Liu, *Magneto-electro-elastic Eshelby tensors for a piezoelectric-piezomagnetic composite reinforced by ellipsoidal inclusions.* Journal of Applied Physics, 1998. **83**(10): p. 5364-5370.
27. Giraud, A., Q.V. Huynh, D. Hoxha, and D. Kondo, *Application of results on Eshelby tensor to the determination of effective poroelastic properties of anisotropic rocks-like composites.* International Journal of Solids and Structures, 2007. **44**(11-12): p. 3756-3772.
28. Lurie, S., D. Volkov-Bogorodsky, A. Leontiev, and E. Aifantis, *Eshelby's inclusion problem in the gradient theory of elasticity: Applications to composite materials.* International Journal of Engineering Science, 2011. **49**(12): p. 1517-1525.
29. Peng, X., S. Tang, N. Hu, and J. Han, *Determination of the Eshelby tensor in mean-field schemes for evaluation of mechanical properties of elastoplastic composites.* International Journal of Plasticity, 2016. **76**: p. 147-165.
30. Le-Quang, H., G. Bonnet, and Q.C. He, *Size-dependent Eshelby tensor fields and effective conductivity of composites made of anisotropic phases with highly conducting imperfect interfaces.* Physical Review B, 2010. **81**(6).
31. Clyne, T.W., *Thermal and Electrical Conduction in Metal Matrix Composites*, in *Comprehensive Composite Materials II*, T.W. Clyne, Editor. 2018, Elsevier. p. 188-212.
32. Clyne, T.W. and P.J. Withers, *An Introduction to Metal Matrix Composites*. Cambridge Solid State Series. 1993, Cambridge: Cambridge University Press.
33. Ashby, M.F. and D.R.H. Jones, *Engineering Materials - An Introduction to Their Properties and Applications*. 1980, Oxford: Pergamon.
34. Evans, R.W. and B. Wilshire, *Introduction to creep*. 1993: Institute of Materials London.

35. Ghoreishy, M.H.R., *Determination of the parameters of the Prony series in hyper-viscoelastic material models using the finite element method.* Materials & Design, 2012. **35**: p. 791-797.
36. Fazekas, B. and T.J. Goda, *Determination of the hyper-viscoelastic model parameters of open-cell polymer foams and rubber-like materials with high accuracy.* Materials & Design, 2018. **156**: p. 596-608.
37. Park, S.W. and Y.R. Kim, *Interconversion between relaxation modulus and creep compliance for viscoelastic solids.* Journal of Materials in Civil Engineering, 1999. **11**(1): p. 76-82.
38. Loy, R.J., F.R. de Hoog, and R.S. Anderssen, *Interconversion of Prony series for relaxation and creep.* Journal of Rheology, 2015. **59**(5): p. 1261-1270.
39. Dean, J., A. Bradbury, G. Aldrich-Smith, and T.W. Clyne, *A procedure for extracting primary and secondary creep parameters from nanoindentation data.* Mechanics of Materials, 2013. **65**: p. 124-134.
40. Dean, J., J. Campbell, G. Aldrich-Smith, and T.W. Clyne, *A Critical Assessment of the "Stable Indenter Velocity" Method for Obtaining the Creep Stress Exponent from Indentation Data.* Acta Materialia, 2014. **80**: p. 56-66.
41. Clyne, B. and J. Campbell, *Testing of the Plastic Deformation of Metals*. 2021.
42. Kartsovnik, V.I., *Changes of Activation Energy during Deformation of Rubber.* Journal of Macromolecular Science Part B-Physics, 2011. **50**(1): p. 75-88.
43. Kartsovnik, V.I., *Prediction of the Creep of Elastomers Taking into Account the Forces of Entropic Elasticity of Macromolecules (Prediction of Creep of Elastomers).* Journal of Macromolecular Science Part B-Physics, 2018. **57**(6): p. 447-464.
44. Standardization, I.O.f., *ISO 7743: 2011: Rubber, Vulcanized Or Thermoplastic. Determination of Compression Stress-strain Properties*. 2011: ISO.
45. Eberlein, R. and R. Kappeler, *Optimisation of nonlinear Material Parameter in uniaxial Compression Tests of Elastomer Specimen involving Friction.* Kgk-Kautschuk Gummi Kunststoffe, 2015. **68**(11-12): p. 33-38.
46. Luo, R.K., X.L. Zhou, and J.F. Tang, *Numerical prediction and experiment on rubber creep and stress relaxation using time-dependent hyperelastic approach.* Polymer Testing, 2016. **52**: p. 246-253.
47. Standardization, I.O.f., *ISO 37: 2011 Rubber, vulcanized or thermoplastic—Determination of tensile stress-strain properties.* 2011.

48. ASTM, D., *2990-01. Standard test methods for tensile, compressive, and flexural creep and creep-rupture of plastics.* West Conshohocken: ASTM International, 2001.
49. Akindoyo, J.O., M.D.H. Beg, S. Ghazali, M.R. Islam, N. Jeyaratnam, and A.R. Yuvaraj, *Polyurethane types, synthesis and applications - a review.* Rsc Advances, 2016. **6**(115): p. 114453-114482.
50. Virgawati, E. and B. Soegijono, *Thermal behaviour and corrosion resistance of nano-ZnO/polyurethane film*, in *3rd International Symposium on Frontier of Applied Physics*, D.S. Khaerudini, et al., Editors. 2018.
51. Soto, M., R.M. Sebastian, and J. Marquet, *Photochemical Activation of Extremely Weak Nucleophiles: Highly Fluorinated Urethanes and Polyurethanes from Polyfluoro Alcohols.* Journal of Organic Chemistry, 2014. **79**(11): p. 5019-5027.
52. Rahimi, A. and A. Mashak, *Review on rubbers in medicine: natural, silicone and polyurethane rubbers.* Plastics Rubber and Composites, 2013. **42**(6): p. 223-230.
53. Michaeli, W., *Extrusion Dies for Plastics and Rubber: Design and Engineering Computations*. 1992: Hanser-Gardner Publications.
54. Nelder, J.A. and R. Mead, *A Simplex Method for Function Minimization.* The Computer Journal, 1965. **7**(4): p. 308-313.
55. Gao, F.C. and L.X. Han, *Implementing the Nelder-Mead simplex algorithm with adaptive parameters.* Computational Optimization and Applications, 2012. **51**(1): p. 259-277.
56. Campbell, J.E., R.P. Thompson, J. Dean, and T.W. Clyne, *Experimental and Computational Issues for Automated Extraction of Plasticity Parameters from Spherical Indentation.* Mechanics of Materials, 2018. **124**: p. 118-131.
57. Clyne, T.W., M.G. Bader, G.R. Cappleman, and P.A. Hubert, *The use of a δ–Alumina Fibre for Metal Matrix Composites.* J. Mat. Sci., 1985. **20**: p. 85-96.
58. Clyne, T.W. and J.F. Mason, *The squeeze infiltration process for fabrication of metal matrix composites.* Metall. Trans., 1987. **18A**: p. 1519-1530.
59. Friend, C.M., *The Effect of Matrix Properties on Reinforcement in Short Alumina Fibre-Aluminium Metal Matrix Composites.* J. Mat. Sci., 1987. **22**: p. 3005-3010.
60. Das, A.A., A.J. Clegg, and B. Zantout. *Enhancement in the Properties of a Squeeze-Cast Aluminium Magnesium Alloy containing Delta-alumina Fibre*. in *Cast Reinforced Metal Composites*. 1988. Chicago: ASM.

61. Taya, M. and R.J. Arsenault, *A Comparison between a Shear Lag type Model and an Eshelby type Model in Predicting the Mechanical Properties of a Short Fibre Composite.* Scripta Met, 1987. **21**: p. 349-354.
62. Withers, P.J., W.M. Stobbs, and O.B. Pedersen, *The Application of the Eshelby Method of Internal Stress Determination for Short Fibre Metal Matrix Composites.* Acta Met., 1989. **37**: p. 3061-3084.
63. Johannesson, B. and O.B. Pedersen, *Analytical determination of the average Eshelby tensor for transversely isotropic fiber orientation distributions.* Acta Materialia, 1998. **46**(9): p. 3165-3173.
64. Small, W., C.T. Alviso, and T.R. Metz, *Gamma Radiation Aging Study of a Dow Corning SE 1700 Porous Structure Made by Direct Ink Writing*, 2015, ; Lawrence Livermore National Lab. (LLNL), Livermore, CA (United States). p. Medium: ED; Size: 12 p.
65. Small, W., M.A. Pearson, A. Maiti, T.R. Metz, E.B. Duoss, and T.S. Wilson, *Thermal Aging Study of a Dow Corning SE 1700 Porous Structure Made by Direct Ink Writing: 1-Year Results and Long-Term Predictions*, 2015, ; Lawrence Livermore National Lab. (LLNL), Livermore, CA (United States). p. Medium: ED; Size: 19 p.
66. Small, W., M.A. Pearson, and T.R. Metz, *Load Deflection of Dow Corning SE 1700 Face Centered Tetragonal Direct Ink Write Materials: Effect of Thickness and Filament Spacing*, 2016, ; Lawrence Livermore National Lab. (LLNL), Livermore, CA (United States). p. Medium: ED; Size: 13 p.
67. Shit, S.C. and P. Shah, *A Review on Silicone Rubber.* National Academy Science Letters-India, 2013. **36**(4): p. 355-365.
68. Amin, M., M. Akbar, and S. Amin, *Hydrophobicity of silicone rubber used for outdoor insulation (An overview).* Reviews on Advanced Materials Science, 2007. **16**(1-2): p. 10-26.
69. Meng, Y., Z. Wei, Y.L. Lu, and L.Q. Zhang, *Structure, morphology, and mechanical properties of polysiloxane elastomer composites prepared by in situ polymerization of zinc dimethacrylate.* Express Polymer Letters, 2012. **6**(11): p. 882-894.
70. Mark, J.E., H.R. Allcock, and R. West, *Inorganic polymers*. 2005: Oxford University Press on Demand.
71. Duoss, E.B., T.H. Weisgraber, K. Hearon, C. Zhu, W. Small, T.R. Metz, J.J. Vericella, H.D. Barth, J.D. Kuntz, R.S. Maxwell, C.M. Spadaccini, and T.S. Wilson, *Three-Dimensional Printing of Elastomeric, Cellular Architectures with Negative Stiffness.* Advanced Functional Materials, 2014. **24**(31): p. 4905-4913.

72. Talley, S.J., B. Branch, C.F. Welch, C.H. Park, J. Watt, L. Kuettner, B. Patterson, D.M. Dattelbaum, and K.S. Lee, *Impact of filler composition on mechanical and dynamic response of 3-D printed silicone-based nanocomposite elastomers.* Composites Science and Technology, 2020. **198**.